Freeze-frame imaging of synaptic activity using SynTagMA

Alberto Perez-Alvarez[1*], Brenna C. Fearey[1*], Ryan J. O'Toole[2], Wei Yang[7], Ignacio Arganda-Carreras[4,5,6], Sabine Hoffmeister-Ullerich[8], Paul J. Lamothe-Molina[1], Benjamien Moeyaert[3], Manuel A. Mohr[3], Lauren C. Panzera[2], Christian Schulze[1], Eric R. Schreiter[3], J. Simon Wiegert[7], Christine E. Gee[1], Michael B. Hoppa[2], Thomas G. Oertner[1§]

[1] Institute for Synaptic Physiology, University Medical Center Hamburg-Eppendorf, Hamburg, D-20251 Germany
[2] Department of Biological Sciences, Dartmouth College, Hanover, NH, 03755 USA
[3] HHMI, Janelia Farm Research Campus, Ashburn VA, 20147 USA
[4]Ikerbasque, Basque Foundation for Science, Bilbao, Spain
[5]Dept. of Computer Science and Artificial Intelligence, Basque Country University, San Sebastian, Spain
[6]Donostia International Physics Center (DIPC), San Sebastian, Spain
[7]Research Group Synaptic Wiring and Information Processing, UKE, Hamburg, D-20251 Germany
[8]Bioanalytics, Center for Molecular Neurobiology Hamburg, UKE, Hamburg, D-20251 Germany

* These authors contributed equally to the study
[§] Corresponding author, thomas.oertner@zmnh.uni-hamburg.de

Abstract

Information within the brain travels from neuron to neuron across billions of synapses. At any given moment, only a small subset of neurons and synapses are active, but finding the active synapses in brain tissue has been a technical challenge. To tag active synapses in a user-defined time window, we developed SynTagMA. Upon 405 nm illumination, this genetically encoded marker of activity converts from green to red fluorescence if, and only if, it is bound to calcium. Targeted to presynaptic terminals, preSynTagMA allows discrimination between active and silent axons. Targeted to excitatory postsynapses, postSynTagMA creates a snapshot of synapses active just before photoconversion. To analyze large datasets, we developed software to identify and track the fluorescence of thousands of individual synapses in tissue. Together, these tools provide a high throughput method for repeatedly mapping active neurons and synapses in cell culture, slice preparations, and *in vivo* during behavior.

INTRODUCTION

The physical changes underlying learning and memory likely involve alterations in the strength and/or number of synaptic connections. On the network level, neuroscience faces an extreme 'needle in the haystack' problem: it is thought to be impossible, in practice, to create a map of all synapses that are active during a specific sensory input or behavior. Although excellent genetically-encoded sensors for calcium, glutamate and voltage have been developed (Adam et al., 2019; Dana et al., 2019; Marvin et al., 2018), and two-photon laser-scanning microscopy enables monitoring the activity of neurons and even single synapses in highly light-scattering brain tissue (Svoboda et al., 1997), the tradeoff between spatial and temporal resolution makes it impossible to simultaneously measure fluorescence in the thousands of synapses of even a single pyramidal neuron. Most functional imaging experiments are therefore limited to cell bodies, i.e. low spatial resolution (Grewe et al., 2010), or monitor the activity of a few synapses within a single focal plane (Iacaruso et al., 2017). Multi-beam scanning designs have been proposed, but due to scattering of emitted photons, they do not produce sharp images at depth (Andresen et al., 2012; Bewersdorf et al., 1998). The need to choose between high temporal or high spatial resolution limits the information we can extract from the brain with optical methods.

A strategy to overcome this limit is to rapidly 'freeze' activity in a defined time window and read it out at high resolution later. The Ca^{2+}-modulated photoactivatable ratiometric integrator CaMPARI undergoes an irreversible chromophore change from green to red when the Ca^{2+} bound form is irradiated with violet (390-405 nm) light (Fosque et al., 2015; Moeyaert et al., 2018). CaMPARI has been successfully applied to map the activity of thousands of neurons in zebrafish, *Drosophila*, and in mouse (Bohra et al., 2018; Fosque et al., 2015; Patel and Cox, 2017; Zolnik et al., 2017). As CaMPARI was designed to diffuse freely within the cytoplasm, it does not preserve subcellular details of Ca^{2+} signaling. By anchoring CaMPARI to either pre- or postsynaptic compartments, we developed tools that mark active synapses in short time windows defined by violet illumination. Three steps were necessary to create a Synaptic Tag for Mapping Activity (SynTagMA): 1) We improved the brightness and conversion efficiency of CaMPARI (Moeyaert et al., 2018); 2) We targeted CaMPARI2 (F391W_L398V) to either presynaptic boutons by fusing it to synaptophysin (preSynTagMA) or to the postsynaptic density by fusing it to an intrabody against PSD95 (Gross et al., 2013) (postSynTagMA); 3) We developed an analysis workflow that corrects for chromatic aberration, tissue displacement (warping) and automatically finds regions of interest (i.e. postsynapses or boutons) to quantify green and red fluorescence. Bouton-localized preSynTagMA allowed us to distinguish active and inactive axons. Spine-localized postSynTagMA allowed us to map the extent of action potential back-propagation into the large apical dendritic tree of hippocampal pyramidal cells. Following repeated sparse activation of Schaffer collateral axons,

postSynTagMA marks a small subset of synapses on CA1 pyramidal cells as highly active. PostSynTagMA is not only useful to analyze the organization of inputs on spiny pyramidal cells, but works equally well for interneurons where most synapses are formed on the dendritic shaft. A fraction of postSynTagMA is sequestered to the nucleoplasm, generating a useful label to identify neurons that are active during a specific behavior. As an application example, we photoconverted active CA1 pyramidal cells during reward collection in a spatial memory task. In summary, the key advantage of SynTagMA compared to acute calcium sensors is the greatly extended read-out period, allowing three-dimensional scanning of relatively large tissue volumes at cellular or at synaptic resolution.

RESULTS

Creating and characterizing a presynaptic marker of activity

To visualize activated presynaptic boutons, we fused the Ca^{2+}-modulated photoactivatable ratiometric integrator CaMPARI (Fosque et al., 2015) to the vesicular protein synaptophysin (sypCaMPARI). In cultured hippocampal neurons, sypCaMPARI showed a punctate expression pattern along the axon, indicating successful targeting to vesicle clusters in presynaptic boutons (**Fig. 1A, F**). CaMPARI fluorescence dims when Ca^{2+} binds (Fosque et al., 2015). Similarly, sypCaMPARI fluorescence decreased after stimulating neurons to evoke trains of action potentials (APs), saturating at 50 APs and slowly returning to baseline (**Fig. 1B-D**). Indeed, the signal-to-noise ratio was sufficient for detecting single APs in single boutons when 30 sweeps were averaged, suggesting a high sensitivity of localized sypCaMPARI for Ca^{2+} influx (**Fig. 1C**). The Ca^{2+}-bound form of CaMPARI is irreversibly photoconverted from a green to a red fluorescent state by 405 nm irradiation (Fosque et al., 2015). Repeatedly pairing electrical field stimulation with 405 nm light flashes increased the red-to-green fluorescence ratio (R/G) of sypCaMPARI boutons in a stepwise fashion (**Fig. 1E and F**). Blocking action potential generation with tetrodotoxin (TTX) strongly reduced photoconversion, indicating that spike-induced Ca^{2+} influx through high-threshold voltage-activated Ca^{2+} channels was necessary for efficient conversion. Similar to the dimming response, the amount of sypCaMPARI photoconversion depended on the number of APs (**Fig. 1G**), suggesting that the R/G ratio can be interpreted as a lasting and quantitative record of axonal activity rather than just a binary signal.

Ca^{2+}-dependent dimming of sypCaMPARI peaked about 1 s after stimulation and returned to baseline after 3-15 s (**Fig. 1B, C**). To determine the photoconversion time window, multiple delays were tested in single experiments using a digital mirror device (**Fig. 2A**). Photoconversion of sypCaMPARI was not efficient when light pulses (100 ms duration) were coincident with stimulation onset (**Fig. 2B, C**). Rather, maximal photoconversion occurred

when violet light was applied 2-5 s after stimulation. The photoconversion window of sypCaMPARI extended to at least 10 s after stimulation, outlasting the dimming response to 5 APs (**Fig. 2B, C, Fig. 1B**). Some photoconversion also occurred in the absence of stimulation or in the presence of TTX (**Fig. 1E, G, 2B, C**). The long temporal window and activity-independent photoconversion are both undesirable traits that limit the utility of sypCaMPARI.

Parallel efforts to improve CaMPARI resulted in CaMPARI2, which contains a number of point mutations improving brightness, increasing kinetics, reducing activity-independent photoconversion and lowering the Ca^{2+} affinity (Moeyaert et al., 2018). We selected the variant CaMPARI2 (F391W_L398V) (K_d Ca^{2+} = 174 nM, k_{on} 66 s^{-1}, k_{off} 0.37 s^{-1}, photoconversion rate in slices 0.22 s^{-1} with Ca^{2+}, 0.0021 s^{-1} without Ca^{2+}) (Moeyaert et al., 2018) and fused it to synaptophysin to create preSynTagMA and expressed it in cultured hippocampal neurons. The temporal precision and dynamic range of preSynTagMA were both enhanced. PreSynTagMA showed no photoconversion in the absence of stimulation and the photoconversion time window was shortened to 0.2 – 2 s post-stimulation, corresponding to the faster dimming in response to 50 APs (**Fig. 2D, E, Fig. S1H**). Using preSynTagMA, we could readily distinguish active from inactive axons in the presence of bicuculline (**Fig. S1A-G**). Blocking action potentials (TTX) completely prevented SynTagMA photoconversion. Two hours after photoconversion, the R/G ratio was still 68% of the peak value, indicating photoconverted preSynTagMA marks activated synapses for at least several hours (**Fig. S1I**). To quantify preSynTagMA localization in tissue, we co-expressed preSynTagMA together with cytosolic mCerulean in hippocampal slice cultures. Using two-photon excitation at 840 nm (mCerulean) and 980 nm (preSynTagMA green) we again observed green fluorescent puncta at axonal boutons (**Fig. 2G**). Compared to mCerulean, preSynTagMA was 4-fold enriched in boutons vs. axonal shafts (**Fig. 2H**).

Targeting SynTagMA to excitatory postsynapses

We chose to target SynTagMA to the postsynaptic protein PSD95, which has a higher retention time than most postsynaptic density proteins (Sturgill et al., 2009). We decided against making a PSD95-CaMPARI fusion protein as overexpression of PSD95 is known to induce dramatic changes in function, size, and connectivity of dendritic spines (Nikonenko et al., 2008). Instead, we fused CaMPARI2 (F391W_L398V) (after deleting the nuclear export sequence) to a genetically encoded intrabody against PSD95 (PSD95.FingR), which provides high specificity without measurable effects on synaptic function (Gross et al., 2013). However, green fluorescence was not limited to dendritic spines, where most excitatory synapses are located, but was detected throughout the dendrites of CA1 pyramidal neurons (**Fig. 3A, D**). We reasoned that the lack of spine enrichment was due to a large fraction of unbound cytoplasmic protein. An elegant method to reduce cytoplasmic fluorescence is to fuse

a zinc finger (ZF) and the transcription repressor KRAB(A) to the targeted protein and include a ZF binding sequence near the promoter (Gross et al., 2013; Margolin et al., 1994). It is presumed that the ZF-KRAB domains direct excess unbound cytosolic protein into the nucleus where the ZF binds to the ZF binding sequence and KRAB(A) suppresses transcription of the exogenous genes. We added these additional regulatory elements to the PSD95.FingR- CaMPARI2 (F391W_L398V) construct, which has no additional nuclear export or localization sequences added, and co-expressed it with mCerulean. Punctate green fluorescence was now observed predominantly in spines and nuclei were fluorescent as expected for a ZF-KRAB(A) containing protein. The ratio of spine-to-dendrite green fluorescence was about 4 times higher than mCerulean spine-to-dendrite ratios, suggesting CaMPARI2 was now localized to postsynapses (**Fig. 3B, E**). Serendipitously, we discovered that the upstream ZF binding sequence was dispensable for autoregulation (**Fig. 3C, F**). We named this simpler construct postSynTagMA and characterized it further. We were concerned there might be widespread suppression of gene expression due to the apparent lack of specificity of the ZF-KRAB(A). We therefore performed qPCR-based expression analysis of 48 endogenous genes in organotypic cultures virus-transduced with postSynTagMA or the construct in Fig. 3A, which is identical but lacking the ZF-KRAB(A) nuclear localization and transcriptional repressor (**Fig. S2**). No RNAs were changed in abundance by more than 2-fold and overall there was also no change in expression (**Fig. 2D**). Furthermore, we blindly measured passive and active electrical properties, miniature excitatory post synaptic currents and spine densities of posSynTagMA expressing neurons and neurons expressing cerulean only (**Fig. S3**). There were no significant differences indicating that expression of postSynTagMA did not alter neuronal physiology during our experiments.

Using back-propagating action potentials to characterize postSynTagMA

We evoked backpropagating action potentials (bAPs) by brief somatic current injections to raise intracellular Ca^{2+}, and applied 395 nm light pulses (500 ms) with a 1 s delay to characterize postSynTagMA photoconversion. In the absence of stimulation (0 bAPs), violet illumination did not change the R/G ratio ($R_1/G_1 = R_0/G_0$). Pairing violet light with bAP trains (15 repeats) lead to increased R_1/G_1 ratios (**Fig 4A**). To determine the best metric for quantifying SynTagMA photoconversion, we plotted several against the initial green fluorescence, which indicates synapse size (**Fig. 4B, Fig. S4A-C**). Considering only the change in red fluorescence ($\Delta R = R_1 - R_0$), the apparent photoconversion positively correlated with synapse size and only large synapses in the 3 bAP and 50 bAP groups could be separated from the non-converted (0 bAP) synapses. The R_1/G_1 ratio, albeit showing better separation than ΔR, negatively correlated with size showing higher values and a higher chance to classify small synapses as photoconverted. When strong photoconversion occurs, small synapses with few indicator molecules may lose all green signal, which is problematic when one wishes to divide by this measure. Evidence of this is

seen in the extremely high values (i.e. 20 - 200) for R_1/G_1, especially in small to medium-sized synapses (**Fig. 4A**). As photoconversion both increases red and decreases green fluorescence, we reasoned that using all channels before and after conversion would provide an optimal metric and avoid dividing by values close to 0. Indeed, $\Delta R/(G_0 + G_1)$ was not correlated with PSD size. Using this measure, we detected a significant increase in photoconversion after 15 x 50 bAPs and even after 15 x 3 bAPs (**Fig. 4C, and 4D**). To test whether violet light had adverse effects on cell health, we performed propidium iodide stainings of cultures exposed to different doses of violet light (**Fig. S5**). The violet light dose used for SynTagMA photoconversion was well below the threshold for photodamage.

Analysis workflow for automatic synapse detection and quantification of SynTagMA

While the efficient targeting of SynTagMA allows simultaneous interrogation of a large population of synapses, it also presents an analysis challenge. To place regions of interest (ROIs) on individual synapses (**Fig. 1 and 2**), simple spot detection algorithms (e.g. Imaris, ImageJ) can be used, but matching of objects across several time points is not straightforward. When the number of synapses reaches into the thousands, a manually curated approach is not feasible. We therefore describe an image analysis workflow to tackle this problem (**Fig. 5**). Images acquired using two-photon excitation at different wavelengths must first undergo correction for laser alignment and chromatic aberration (**Fig. 5A**). As synapses in tissue are quite motile even on short time scales (Bonhoeffer and Yuste, 2002; Fischer et al., 1998), a non-rigid 3D transformation, termed 'unwarping', was applied to re-align and preserve synapse identity across time points. To achieve the highest quality transformation, images were first deconvolved and then underwent 'unwarping' (**Fig. 5B-C**). Synapses were then detected on transformed datasets using the Spot feature of Imaris (Oxford Instruments) (**Fig. 5D**). Although each of these steps can be performed using a combination of freely and commercially available software packages, it is a time-consuming process that generates several gigabytes of data in intermediate steps. We therefore developed SynapseLocator (available at GitHub), a Matlab-based program with a user interface to streamline these aforementioned steps using freely available ancillary software tools (Fiji (Schindelin et al., 2012), DeconvolutionLab2 (Sage et al., 2017), FeatureJ, elastix (Klein et al., 2010)). A machine-learning approach (Arganda-Carreras et al., 2017) was implemented to generate synapse templates (boutons or postsynaptic sites) that were used to automatically detect and extract fluorescence values by SynapseLocator. Transformed images and fluorescence values from identified synapses (ROIs) were saved for statistical analysis and imported into ImageJ or Imaris for 3D visualization (**Fig. 5D**). A specific difficulty for automated analysis is the presence of spot-like red autofluorescence at 1040 nm excitation. Synapses with elevated R_0/G_0 values at baseline were considered too close to autofluorescent objects and were automatically excluded from further analysis.

Automation of the synapse identification process greatly reduced the analysis time (from days for ~500 hand-curated ROIs at several time points to minutes for ~4000 automatically detected ROIs from the same dataset, using a personal computer). Manual and automated analysis produced comparable results (**Fig. S6**).

Back-propagating action potentials increase Ca^{2+} at proximal synapses

For a given number of bAPs, the amount of photoconversion was quite variable between individual spines (**Fig. 4A**), likely reflecting spine Ca^{2+} transients of different amplitude and duration. We also observed that whereas synapses close to the soma were strongly photoconverted, conversion decreased with distance, suggesting that bAP bursts do not increase [Ca^{2+}] in distal branches of the apical dendrite (**Fig. 5E and 5F, Supplemental Movie 1**). To test whether SynTagMA conversion is a linear reporter of local Ca^{2+} signal amplitude, we performed equivalent experiments on CA1 neurons expressing jGCaMP7b. Indeed, Ca^{2+} imaging during trains of bAPs yielded the same exponential decay of amplitude as a function of distance from the soma validating our observation that bursts of bAPs do not invade distal dendrites (**Fig. 5G**). In contrast to imaging Ca^{2+} synapse-by-synapse, postSynTagMA photoconversion reliably reports the amplitude of bAP-induced Ca^{2+} elevations across the entire dendritic tree, resulting in higher coefficients of determination (R^2) in the statistical analysis (R^2 = 0.91 vs 0.66).

Using postSynTagMA to map synaptic activity

Having established the linear Ca^{2+}-dependence of photoconversion in patch-clamped CA1 neurons, we next wanted to assess how long converted postSynTagMA would persist in individual spines. We illuminated rectangular areas of cultured neurons while stimulating the culture at 50 Hz, limiting postSynTagMA photoconversion to the illuminated dendritic sections (**Fig. 6A**). We observed that $\Delta R/(G_0 + G_t)$ returned to baseline with a time constant of 29 min, in contrast to the much slower turnover of preSynTagMA (**Fig. S1I**) and of photoconverted soluble CaMPARI (Moeyaert et al., 2018). This relatively fast decay of the spine signal, which is consistent with the short retention time of synaptic PSD95 in the neocortex of young mice (Gray et al., 2006), limits the post-photoconversion acquisition time to about 30 minutes. On the other hand, rapid turnover enables multiple rounds of photoconversion, i.e. activated synapses can be remapped in a relatively short time span. Indeed, using electrical stimulation of Schaffer collateral axons in organotypic slice culture, we were able to convert (median $\Delta R/(G_0 + G_1)$ = 1.26) and, 18 hours later, reconvert (median $\Delta R/(G_0 + G_1)$ = 1.25) SynTagMA-labeled spines on CA1 pyramidal cells, suggesting that multiple activity maps are feasible with postSynTagMA (**Fig. 6B**). However, as the postsynaptic neuron may have been spiking in these experiments, we could not distinguish spines that received direct synaptic input from spines that were passively flooded with Ca^{2+} (**Fig. 6C**).

We next tested whether subthreshold synaptic stimulation would sufficiently raise Ca^{2+} to photoconvert and mark active synapses with postSynTagMA. Violet light (100 ms) was applied 1 s after evoking sub-threshold synaptic responses in CA1 pyramidal cells (15-25 mV or -500 to -1000 pA), which assuming unitary responses of 0.9 mV or -18 pA (Debanne et al., 1995) would mean 20-50 active synapses. In a 65 x 65 x 78 μm^3 volume containing a proximal region of the apical dendritic tree, we detected and analyzed 1500 postSynTagMA labeled synapses (**Fig. 6D, Supplemental Movie 2**). Fourteen spines showed values above 3 σ ($\Delta R/(G_0 + G_1) = 0.97$) and were therefore classified as active (**Fig. 6D**). This number is consistent with our expectations considering that we imaged approximately 10% of the entire dendritic tree (Bannister and Larkman, 1995; Megías et al., 2001). To have an independent marker of synaptic activation, we stimulated presynaptic CA3 neurons expressing channelrhodopsin2 ET/TC (ChR2) and synaptophysin-mCerulean by blue light pulses (Berndt et al., 2011). Next to the most strongly photoconverted spines, cyan fluorescent boutons were observed, suggesting that these synapses were directly innervated and activated by ChR2-expressing presynaptic CA3 neurons (**Fig. S4).** Non-photoconverted spines were also distant from activated terminals and thus represent 'true negatives' **(Supplemental Movie 3**). A potential problem for synaptic mapping is the conversion of postSynTagMA by back-propagating APs. To address this concern, we went to the molecular layer of dentate gyrus, where granule cell dendrites radiate and receive excitatory inputs in a strictly layered fashion. Illumination during electrical stimulation of the inner molecular layer photoconverted synapses in that layer, but not synapses along the dendrites in the outer two-thirds of the molecular layer (**Fig. 6E and F**). Thus, photoconversion by bAPs was negligible; otherwise we would have detected photoconverted objects on distal dendritic branches of the electrotonically compact granule cells.

PostSynTagMA maps active neurons and synapses *in vivo*

The nuclear sequestration of postSynTagMA prompted us to test whether it could be used to identify active neurons *in vivo*. When a head-fixed mouse running on a linear treadmill was illuminated with 405 nm light, a small percentage of the CA1 neuronal nuclei expressing postSynTagMA turned red (**Fig. 7A**). In the same mouse, there was no photoconversion during ketamine-xylazine anesthesia (**Fig. 7B**), consistent with the strongly reduced activity levels (**Supplemental Movie 4**). We next trained mice to stop and receive a water reward at a particular location (**Fig. 7C-D**). After reaching criterion, we monitored green fluorescence continuously during four laps (**Fig. 7E and 7F**), followed by 15 laps with reward-triggered light. The neurons that were photoconverted also showed dimming (i.e. increased Ca^{2+}) immediately prior to each reward (**Fig. 7F,** magenta) whereas a matched number of randomly selected non-converted neurons did not (**Fig. 7F,** green). Therefore, in awake behaving animals, postSynTagMA photoconversion selectively labels neurons with high calcium

transients (**Supplemental Movie 5**). The density of neuropil labeling in these mice prompted us to switch to expressing postSynTagMA in interneurons (**Fig. S7**) to test whether postSynTagMA could be used to identify individual active synapses/dendrites in sparsely labeled neurons in vivo. We photoconverted sparsely labeled interneurons in *stratum oriens* interneurons under isoflurane anesthesia which retains neuronal activity at close to awake levels but reduces motion artifacts (**Fig. 7G-H, Supplemental Movie 4**). Photoconversion of clusters of synapses was observed, which would be consistent with local dendritic calcium events that have been described in interneurons in vivo (Francavilla et al., 2019). Thus, under conditions of sparse SynTagMA expression, it is possible to resolve individual photoconverted synapses *in vivo*. During photoconversion, movement of the brain is not problematic and SynTagMA can be used to tag active neurons and synapses during behavior. To later resolve the SynTagMA label at the level of individual synapses, minimizing tissue movements with anesthesia may improve data quality.

DISCUSSION

To create a synaptically localized, photoconvertible calcium sensor, we fused CaMPARI2 to the vesicle protein synaptophysin (preSynTagMA) for presynaptic targeting or to a nanobody against the postsynaptic scaffold of excitatory synapses (postSynTagMA). Both targeting strategies have previously been used to label synapses with fluorescent proteins (Gross et al., 2013; Li and Murthy, 2001), and we verified that the autoregulatory elements of postSynTagMA do not cause widespread misregulation of endogenous gene expression and that SynTagMA-expressing neurons are physiologically normal. When SynTagMA is combined with a second fluorescent protein, here mCerulean, postSynTagMA puncta can be assigned to particular dendrites or neurons. PreSynTagMA should prove useful for identifying active axons in tissue and may also prove useful for distinguishing high from low release probability boutons based on the graded photoconversion. PostSynTagMA should likewise facilitate identification and mapping of active synapses, but on the postsynaptic side. Antibodies specific to the photoconverted red form will also enable further ultrastructural analysis of the marked synapses (Moeyaert et al., 2018).

Identifying active synapses is a long-standing quest in neuroscience and many approaches have been put forward. In two-dimensional neuronal cultures, it is relatively straightforward to monitor the activity of a large number of synapses with a high speed camera, e.g. by employing genetically encoded sensors of vesicular pH (Ariel and Ryan, 2010; Miesenbock et al., 1998). In intact brain tissue, however, monitoring more than one synapse with high temporal resolution becomes very challenging (Dürst et al., 2019; Iacaruso et al., 2017). To create a more permanent tag of active synapses, Ca^{2+} precipitation in active spines was used to create an electron-dense label that can be detected by electron microscopy (Toni et al., 1999). As this method requires

tissue fixation, it does not allow monitoring changes in synaptic activity over time. Expressing the two halves of split-GFP on the extracellular surface of pre- and postsynaptic neurons (mGRASP) labels contact points between the neurons as green fluorescent puncta (Feinberg et al., 2008). Refined transsynaptic labeling methods with multiple colors have led to remarkable insights about network connectivity (Choi et al., 2018; Macpherson et al., 2015). Whereas mGRASP and eGRASP report anatomical proximity, SynTagMA photoconversion is Ca^{2+}-dependent and therefore sensitive to synaptic activity.

One of the many interesting applications of postSynTagMA will be to create extensively detailed input maps of individual neurons at single synapse resolution. The question of whether inputs carrying similar information segregate to branches of the dendritic tree is currently being investigated using spine-by-spine Ca^{2+} imaging (Chen et al., 2011; Iacaruso et al., 2017; Scholl et al., 2017). By freezing the activity status of all spines during a particular labelling protocol, SynTagMA may simplify such experiments by reading out fluorescence ratios in thousands of spines in a single high-resolution stack. Importantly, postSynTagMA maps can be repeated, opening the possibility to study the functional dynamics of excitatory connections rather than just morphology and turnover of dendritic spines. In addition to synapses on mushroom-shaped spines, postSynTagMA provides access to synapses on structures that are difficult to probe with Ca^{2+} dyes or diffusible GECIs, such as stubby spines or shaft synapses (Soler-Llavina and Sabatini, 2006). Thus, postSynTagMA may open the possibility to study the long-term dynamics of interneuron excitation, a key homeostatic mechanism that involves Ca^{2+}-induced-Ca^{2+} release from intracellular stores (Topolnik and Camiré, 2019). In addition to Ca^{2+} influx though voltage- or ligand-gated channels, Ca^{2+} release is thought to be important in both presynaptic (de Juan-Sanz et al., 2017) and postsynaptic compartments (Emptage et al., 1999; Holbro et al., 2009; Sabatini et al., 2002), and SynTagMA may help investigating the sources of Ca^{2+} in individual synapses.

To test the linearity of calcium-dependent photoconversion, we used bursts of action potentials (APs) which are known to be strongly attenuated on their way into the dendrite (Golding et al., 2001; Spruston et al., 1995). Indeed, postSynTagMA photoconversion was greatest in spines relatively close to the soma while distal synapses were not converted at all. The distance constant estimated from a Sholl analysis of postSynTagMA conversion (λ = 105 µm, **Fig. 5F**) was the same as that determined by calcium imaging of individual spines (λ = 106 µm, **Fig. 5G**). Previous studies (Golding et al., 2001; Spruston et al., 1995) have measured back-propagation along the apical dendrite, but not along thin oblique dendrites or into individual spines. Studies with single-spine resolution (Holbro et al., 2010; Yasuda et al., 2003) have not included large-scale spatial information, as only few synapses per cell can be investigated. In future SynTagMA studies, reconstructions of the neuronal morphology in 3D would allow accurate measurements of the dendritic path length to every synapse and combine that data

with functional information. We observed that even close to the soma, conversion of spines was not very uniform and the same was true for boutons. Understanding the sources of this heterogeneity, and whether these correspond to particular classes of synapses, may lead to important insights into synapse-specific calcium regulation.

An unexpected application arose from the nuclear localization of postSynTagMA. As we show, nuclear SynTagMA conversion can be used to visualize the location of the most active neurons in behaving animals. As the cytoplasm is almost free of label, automatic segmentation is very easy. Nuclear calcium elevations may be of particular relevance during learning, as they are driven by burst firing and trigger transcription of plasticity-related genes (Yu et al., 2017). There are already several strategies for labeling active neurons (DeNardo and Luo, 2017), but their time resolution is much worse than the 2 s photoconversion time window of SynTagMA.

There are some caveats to working with SynTagMA. Before or during imaging, it is important to photoswitch the protein to the bright state using low intensity violet light (Fosque et al., 2015; Moeyaert et al., 2018). The quite rapid turnover of postSynTagMA means that after photoconversion, images should be collected within about 30 minutes. SynTagMA analysis is complicated by endogenous red fluorescence which can be mistaken for photoconverted SynTagMA. For this reason, we found acquisition of a pre-photoconversion stack essential for reliable analysis: Synaptic ROIs (detected in the green channel) that already show elevated red fluorescence *before* stimulation (large R_0/G_0) can be classified as 'contaminated' and excluded from further analysis (see **Fig. 7G** for example red "spots" in both pre- and post-photoconversion images). If for experimental reasons only a single time point can be acquired, we recommend excluding objects that have high red fluorescence in the voxels surrounding green puncta. When acquiring two-photon image stacks, we collected each optical section twice, exciting either the green or the red form of SynTagMA by rapidly switching the power of two different Ti:Sapph lasers. Near-simultaneous acquisition of red and green fluorescence prevented movement artefacts and made it straightforward to correct for chromatic aberration. When the two color channels are collected in successive stacks, Ca^{2+}-dependent dimming driven by spontaneous activity may affect one and not the other channel. Particularly when imaging in vivo, the time required to re-tune a single laser to the different excitation wavelengths might make analysis of individual synapses impossible.

If the postsynaptic neuron fires APs during strong (supra-threshold) synaptic activation, the resulting global calcium elevation could interfere with SynTagMA-based input mapping at proximal synapses. As we show, this is much less of a problem in the distal dendritic tree. For input-mapping experiments, it is advisable to repeat weak, subthreshold stimuli many times, each time paired with a (delayed) pulse of violet light. To avoid phototoxicity, it is important to keep track of the total light dose applied during each protocol, using shorter

pulses (or lower light intensities) for protocols with many repetitions. For example, 15 x 500 ms pulses at 16 mW mm^{-2} = 0.12 J mm^{-2} (**Fig. 4**); 50 x 100 ms pulses at 16 mW mm^{-2} = 0.8 J mm^{-2} (**Fig. 6C, D, Fig. S5**).

SynTagMA is amenable for viral delivery using recombinant AAVs. Using different promoters, we demonstrate strong and sparse expression of postSynTagMA in hippocampal interneurons and pan-neuronal expression for network analysis (**Fig. 7**). For sparse expression in pyramidal cells, dual-AAV labeling systems could be employed (Lin et al., 2018).

AUTHOR CONTRIBUTIONS

Conceptualization, TGO, CEG, MH and SW; **Methodology**; **Software** CS, IAG; **Investigation**, APA, BCF, RJO, WY, SFU, PLM, BM, MAM, LCP, JSW, MBH; **Resources** ERS; **Writing – Original Draft,** CEG, TGO, MBH, JSW, BCF, APA, CS, SFU; **Writing – Review & Editing**, APA, BCF, RJO, WY, IAC, SHU, PLM, BM, MAM, LCP, CS, ERS, JSW, CEG, MBH, TGO; **Visualization,** BCF, APA, CS, TGO, MBH; **Supervision** ERS, JSW, CEG, MBH, TGO; **Project Administration** CEG; **Funding Acquisition**, ERS, JSW, CEG, MBH, TGO.

ACKNOWLEDGEMENTS

We thank Iris Ohmert, Sabine Graf and Kathrin Sauter for excellent technical assistance. Dr. Ingke Braren of the UKE Vector Facility produced AAV vectors. mCerulean was kindly provided by Dr. Wolfgang Wagner at the ZMNH. PSD95.FingR was kindly provided by Dr. Don Arnold at USC. Synaptophysin-GCaMP3 was kindly provided by Loren Looger at Janelia Farm. Funding was received from: The Deutsche Forschungsgemeinschaft (DFG) grants SPP 1665 220176618, SPP1926 273915538, SFB 936 178316478, SFB 1328 335447717, FOR 2419 278170285; the European Research Council (ERC-2016-stG 714762); the National Institute of Health (GM13132); the Howard Hughes Medical Institute. BCF was supported by an individual fellowship from the DAAD (Research Grants - Doctoral Programmes in Germany, 57214224). RJO was supported by the Esther and Joseph Klingenstein-Simons Foundation (FP00003669) and U.S. Department of Education GAANN grant (P200A150059). LCP was supported by NSF IOS grant 1750199. BM holds a postdoctoral fellowship from the Research Foundation-Flanders (FWO Vlaanderen)

MAIN FIGURES

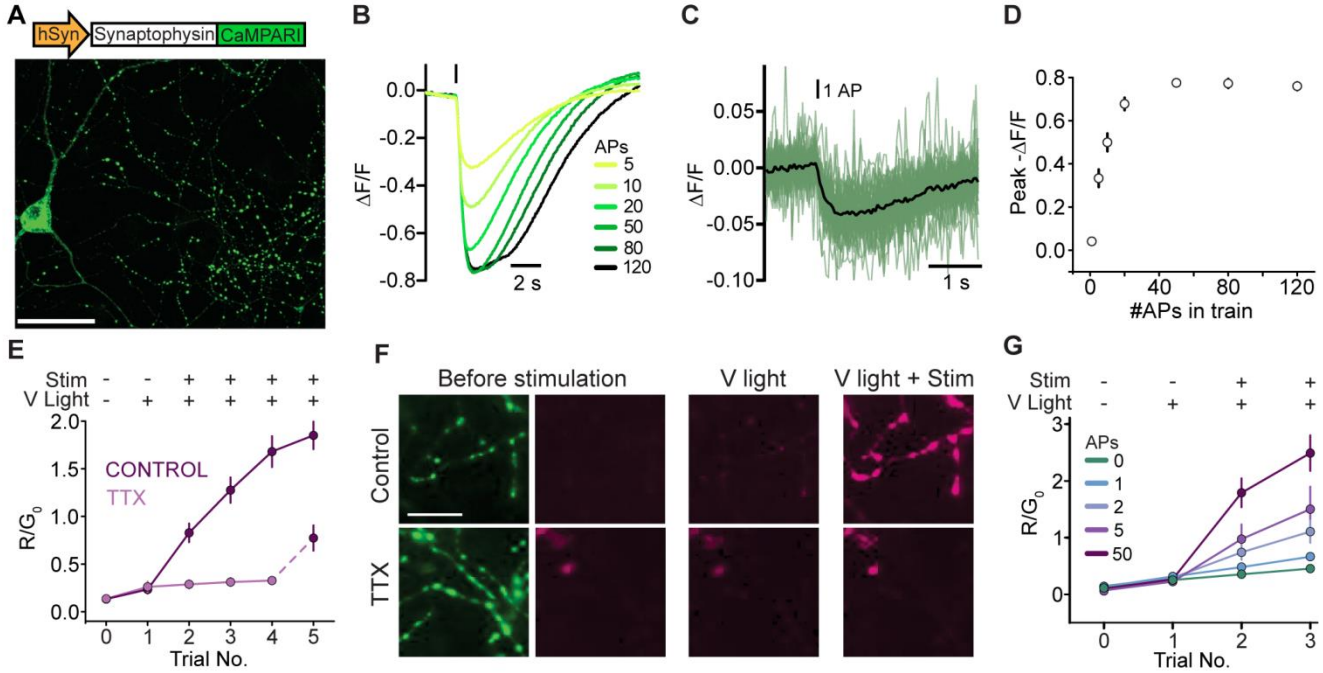

Figure 1 | Synaptophysin-fused CaMPARI marks active presynaptic terminals. (A) Representative image of cultured rat hippocampal neurons expressing sypCaMPARI showing punctate labeling in axonal boutons. Scale bar 50 µm. **(B)** Average fluorescence response of sypCaMPARI boutons (green channel emission) to varying numbers of action potentials (APs) evoked at 50 Hz (n = 6 neurons). **(C)** Trial-averaged responses to 30 single APs (green, n = 57 boutons). Black line is the average, representative of n = 3 neurons. **(D)** Plot of the maximum ΔF/F versus number of APs from the experiments in B) and C) (n = 6 cells, 317 synapses). **(E)** Plot of initial red to green ratio of boutons expressing sypCaMPARI (R_0/G_0, V light -, Stim -), after photoconverting violet light alone (405 nm, 20 flashes x 1 s, 0.1 Hz, 10.8 mW cm^{-2}, V light +, Stim -) and after simultaneous stimulation with trains of 50 APs at 50 Hz (V light +, Stim +, repeated 4 times). The experiment was performed in the absence or presence of 3 µM tetrodotoxin to block action potentials (control: n = 8 cells; TTX: n = 7 cells). Note that after washing out TTX, the R/G_0 ratio (V light + Stim +, trial 5) increased to the same extent as the first instance in control neurons (trial 2). **(F)** Representative red (magenta, Trial 0, Trial 1, Trial 3) and green (green, Trial 0) images of boutons from the experiment in E). The scale bar 20 µm applies to all panels in F. **(G)** The amount of photoconversion (R/G_0) in a similar experiment as E) but varying the number of APs in a 50 Hz train (V light 405 nm, 20 flashes x 1 s, 0.1 Hz, 54.1 mW cm^{-2}, Stim 20 bursts at 50 Hz). Data are mean ± SE (0 AP: n = 4 cells, 1 AP: n = 4, 2 APs: n = 5, 5 APs n = 5, 50 APs n = 7). 50 AP fold increase was statistically different from all other stimulation conditions using a one-way ANOVA with Tukey's post-hoc comparison ($p < 0.05$).

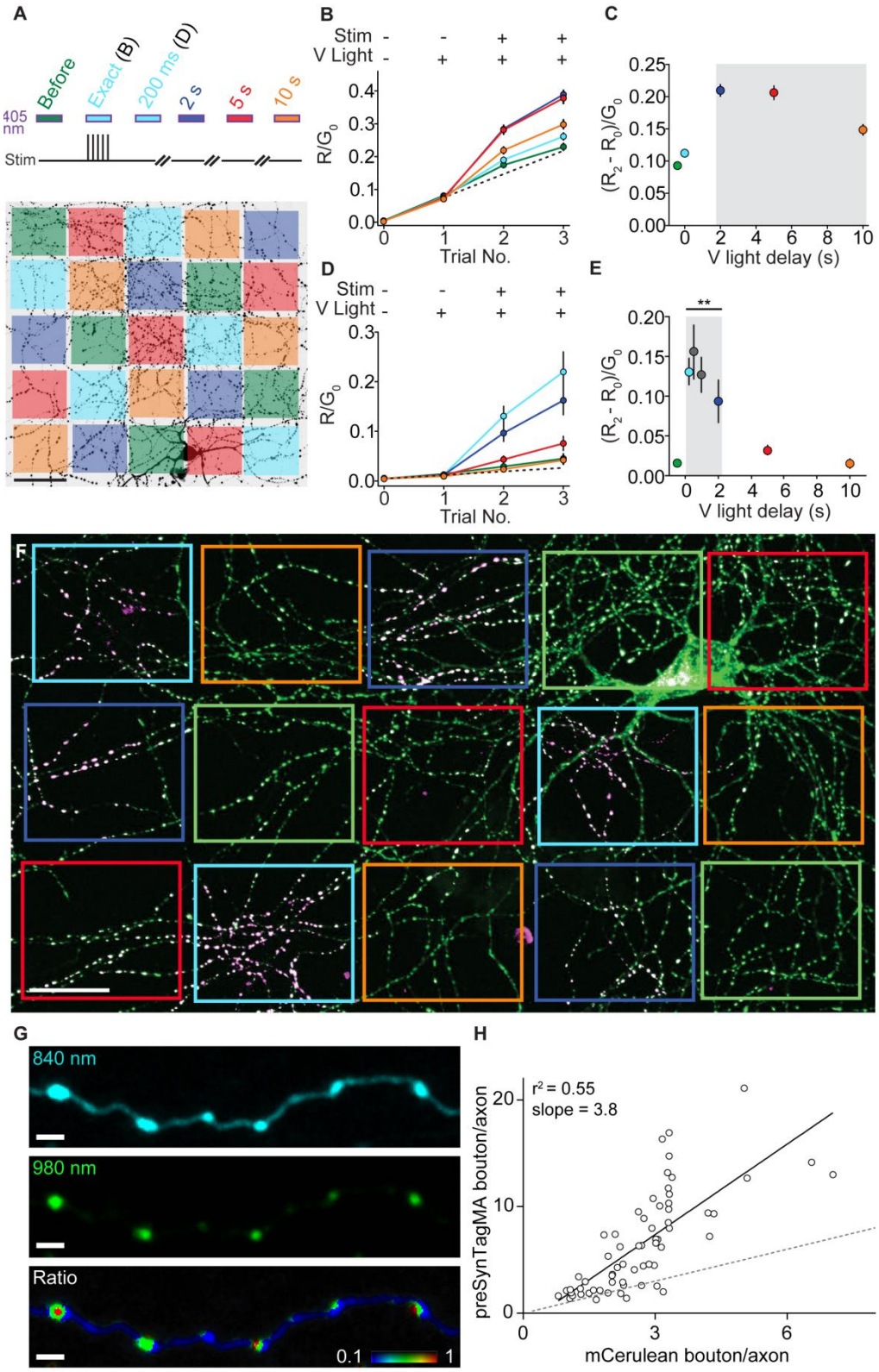

Figure 2 | Improved resolution of presynaptic SynTagMA. (A) Experimental design: Initial red (R_0) and green (G_0) fluorescent images were acquired of cultured rat hippocampal neurons. A computer-controlled spatial light modulator was used to apply timed photoconverting violet light (405 nm, 50 mW cm^{-2}) alone or at different time

intervals relative to 5 APs @ 50 Hz in a grid pattern over the axonal arbor (repeated 5x, 30s intervals). After each trial, new images were acquired and red fluorescence intensity ($R_{Trial\ No.}$) compared to the G_0. Note that both 'exact' & '200 ms' timing are cyan. sypCaMPARI experiments used 'exact' and preSynTagMA used '200 ms' timing in the cyan quadrant. **(B)** Ratio of red to green fluorescence (R/G_0) from sypCaMPARI boutons illuminated with various delays alone (Stim -, V light +, Trial 1) or together with APs (Stim +, V light +, Trial 2, 3). Lines have the same color code as panel A), n = 6 cells **(C)** Activity-dependent photoconversion ($\Delta R/G_0$) versus delay from start of stimulation to violet light from experiments in b). The grey box indicates the long time window (up to 10 s after activity) for efficient photoconversion of sypCaMPARI. **(D)** Neurons expressing preSynTagMA (synaptophysin-CaMPARI2 (F391W, L398V)) were stimulated as in A-C. Note the greatly reduced increase in R/G_0 with violet light alone. n = 6 cells **(E)** Activity-dependent photoconversion ($\Delta R/ G_0$) versus delay of preSynTagMA expressing neurons. The grey box indicates the much shorter time window (200 ms to 2 s after activity) for efficient photoconversion of SynTagMA. n = 12 cells total, 12 pre, 12 200 ms, 6 500 ms, 6 1 s, 12 2 s, 6 5 s, 6 10 s. **(F)** Cropped example of cultured rat hippocampal neurons expressing preSynTagMA after trial 3. Boxes indicate regions where photoconversion light was applied with different delays (color code as in panel A). **(G)** Two-photon images of axonal boutons in CA1 *stratum radiatum* originating from CA3 neurons expressing preSynTagMA and mCerulean as cytosolic filler (hippocampal slice cultures). Upper panel shows mCerulean fluorescence (excited at 840 nm), middle panel is preSynTagMA fluorescence (excited at 980 nm), lower panel is the ratio image. **(H)** The ratio of preSynTagMA bouton to axonal shaft fluorescence vs the ratio of mCerulean bouton to axon fluorescence for n = 64 boutons. Solid line is the linear fit to the data points, dashed line (slope = 1) indicates the theoretical 'no bouton enrichment' fit. Data in B-E) are presented as mean ± SE. Statistics were performed using Kruskal-Wallis ANOVA followed by Dunn's multiple comparison ** $p < 0.01$ vs pre. Scale bars: A) 50 µm, F) 25 µm, and G) 2 µm.

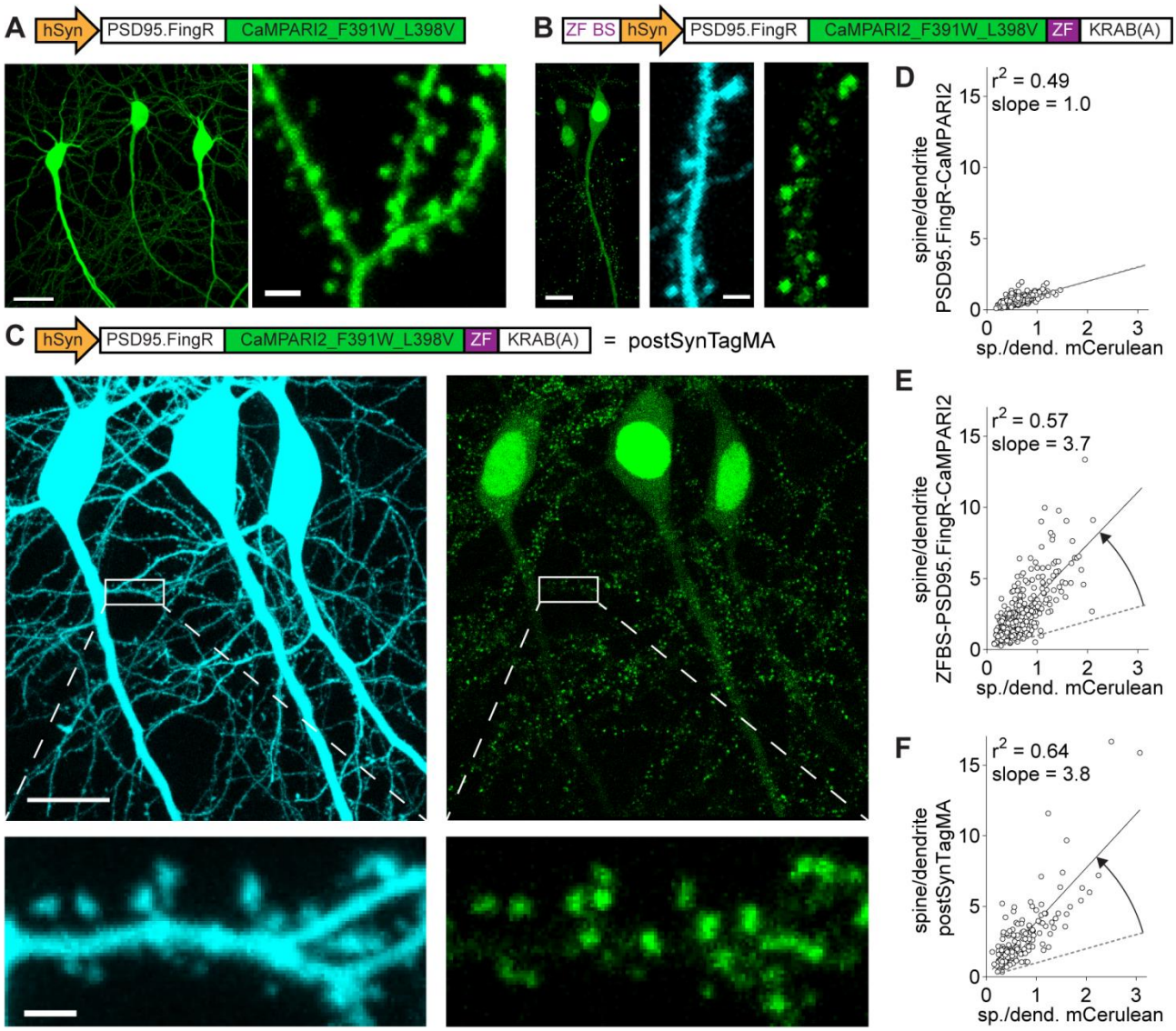

Figure 3 | Postsynaptic targeting of SynTagMA using a PSD95 intrabody. (**A**) Two photon maximum intensity projection (excitation 980 nm) from CA1 neurons expressing a fusion protein of PSD95 fibronectin intrabody (PSD95.FingR) and CaMPARI2_F391W_L398V (without NES or epitope tags). Scale bars 20 µm, 2 µm respectively. (**B**) Two photon maximum intensity projections from a CA1 neuron expressing PSD95.FingR-CaMPARI2 with a zinc finger binding sequence (ZF BS) added upstream of the promoter and a zinc finger (ZF) fused to a transcriptional repressor domain (KRAB(A)) and mCerulean (excitation 840 nm). Plotted is the spine to dendrite green fluorescence ratio vs the cyan spine to dendrite ratio (1 slice, 3 neurons, 367 spines). Scale bar 12 µm (left panel) and 2 µm (center and right panels). (**C**) Postsynaptically targeted SynTagMA (postSynTagMA). As in b) with the ZF-KRAB(A) but no upstream ZF-BS. Note that postSynTagMA is still enriched in spines and the nucleus, leaving the cytoplasm almost free of SynTagMA (2 slices, 3 neurons, 179 spines). Scale bars: upper 20 µm, lower 2 µm. **(D)** The unregulated construct is expressed at high levels, leading to near-identical concentrations in dendrites and spines (same as freely diffusible mCerulean). (**E**) The construct with autoregulatory elements shuts off its own production, resulting in strong enrichment in spines (compared to freely diffusible mCerulean). (**F**) The construct without zinc finger binding sequence (postSynTagMA) is also auto-regulated, showing equally strong enrichment in spines.

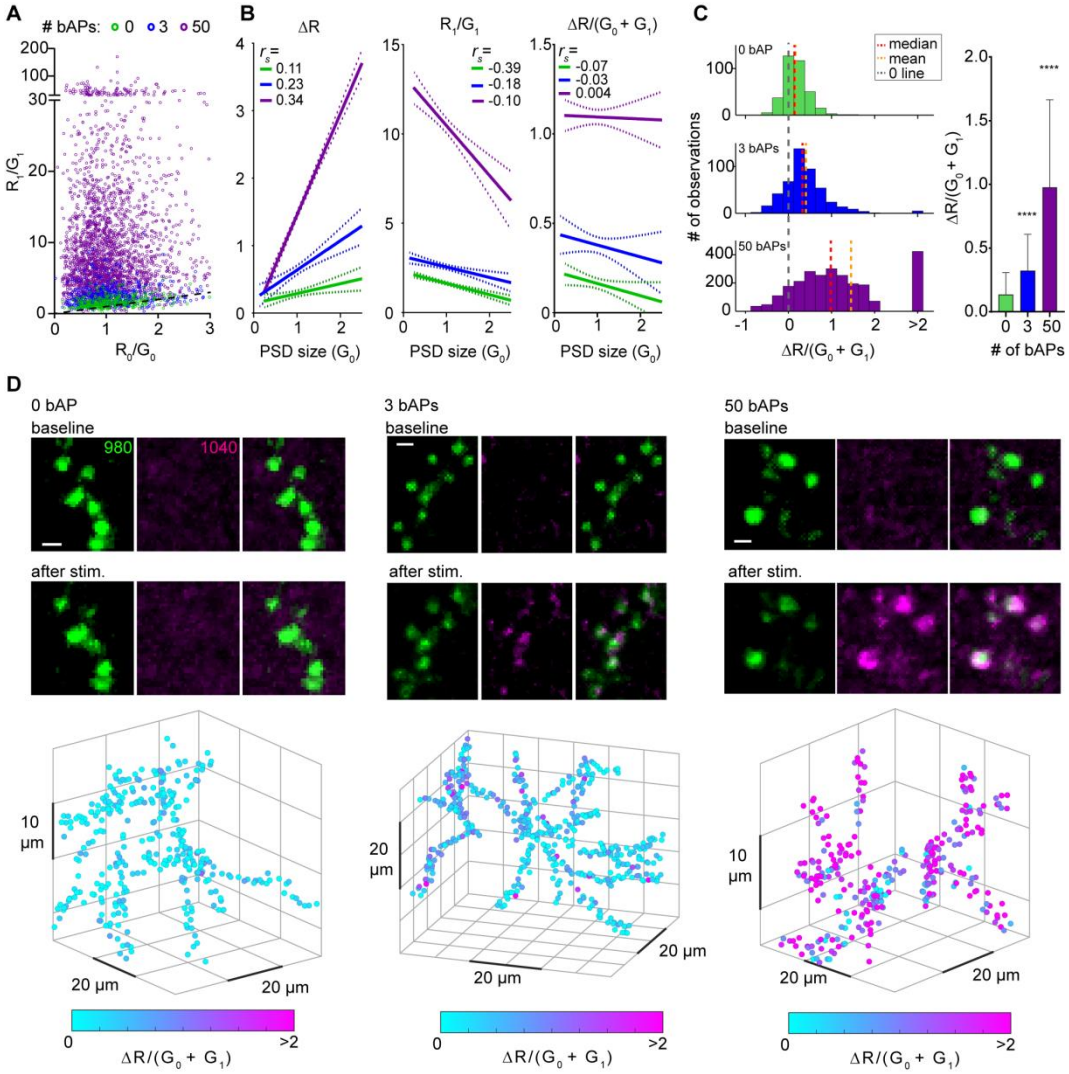

Figure 4 | PostSynTagMA photoconversion with back-propagating action potentials (bAPs). Two-photon image stacks of postSynTagMA expressing CA1 pyramidal neurons (excitation 980 nm and 1040 nm) were taken before and after 15 pairings of trains of bAPs (100 Hz) with photoconverting violet light (395 nm, 16 mW mm^{-2}, 500 ms duration, 1 s delay). Synaptic transmission was blocked. **(A)** R/G ratios of individual synapses before (R_0/G_0) vs after (R_1/G_1) photoconversion. Note the variability in photoconversion within conditions. Dotted black line is the unity line. **(B)** Three different metrics vs PSD size (Magenta: 50 bAPs. Blue: 3 bAPs. Green: 0 bAP; linear regression lines with 95% confidence intervals). ΔR is positively correlated with PSD size (0 bAPs: $r_s = 0.11$, p = 0.03; 3 bAPs: $r_s = 0.23$, p < 0.0001; 50 bAPs: $r_s = 0.34$, p < 0.0001). Normalizing ΔR by ($G_0 + G_1$) removes the correlation with PSD size (0 bAP: $r_s = -0.07$, p = 0.164; 3 bAPs: $r_s = -0.03$, p = 0.583; 50 bAPs: $r_s = 0.004$ p = 0.876). r_s is the correlation coefficient (Spearman's rho). **(C)** Distributions of photoconversion ($\Delta R/(G_0+G_1)$) for each condition (0 bAP: median = 0.139, mean = 0.164; 3 bAPs: median = 0.327, mean = 0.406; 50 bAPs: median = 0.984, mean = 1.452) and $\Delta R/(G_0+G_1)$ vs the number of bAPs (data are median and interquartile range; ****p < 0.0001, Kruskal-Wallis vs. 0 bAP). 0 bAP: n = 1 cell, 356 synapses; 3 bAPs: n = 1 cell, 472 synapses; 50 bAPs: n = 3 cells, 2587 synapses. **(D)** Example green, red and merged images of SynTagMA labelled spines photoconverted with 0, 3 or 50 bAPs. Below the color-coded photoconversion factor of individual spines vs their 3D-positions in the dendritic arbor are plotted. Spines with values 2 and above are all magenta color. Scale bars 1 µm.

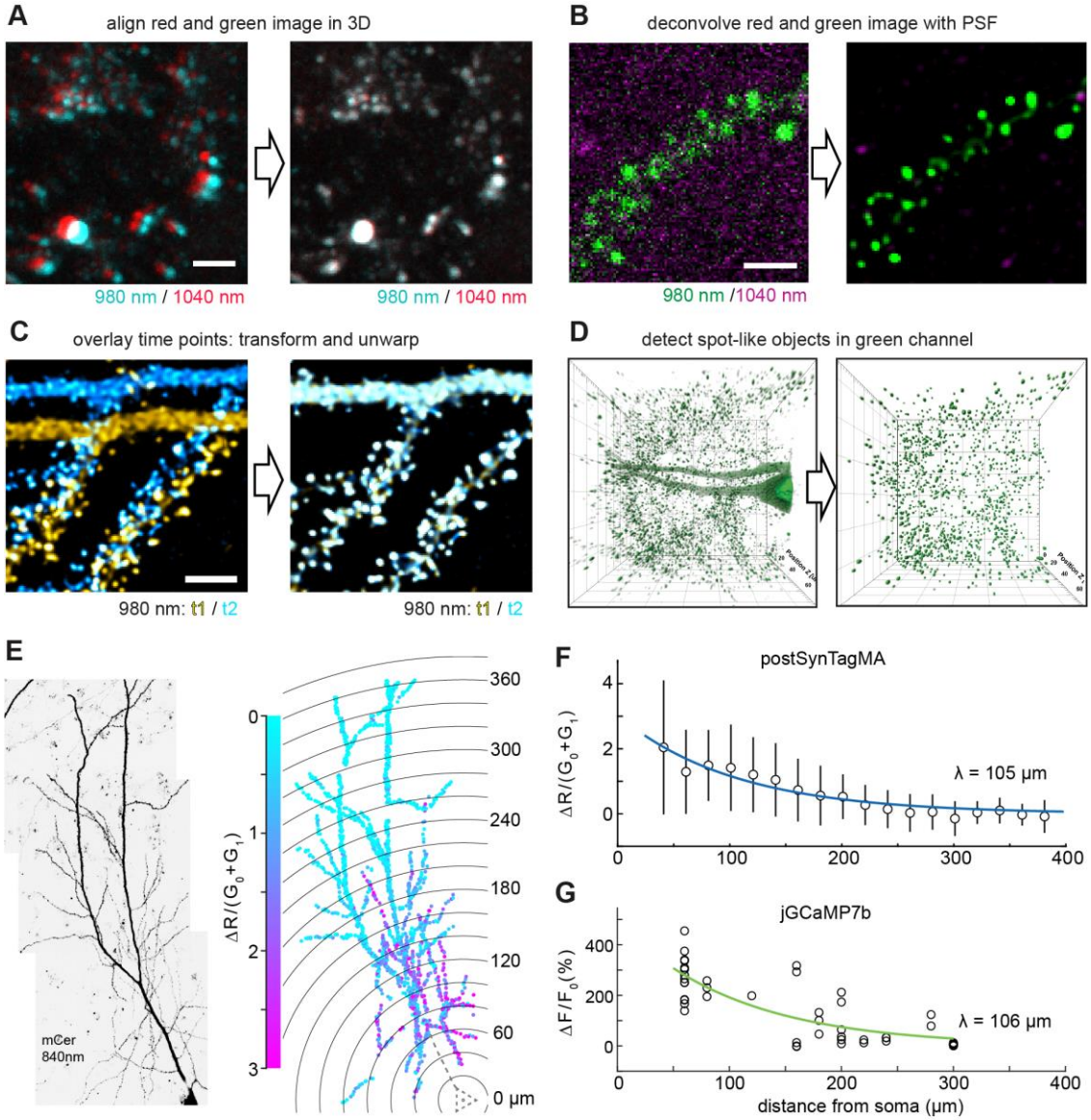

Figure 5 | Analysis workflow for automated detection and analysis of SynTagMA photoconversion. (A) Green and red fluorescence is collected in separate images, switching between two Ti/Sapph lasers (980 nm / 1040 nm). Images are registered in 3D to correct for chromatic aberration and laser alignment. Scale bar: 4 µm. **(B)** Median filtering and deconvolution is then applied to all images (both green and red channel). Scale bar: 3 µm. **(C)** To superimpose multiple time points in 3D, transformations (translation/rotation) and unwarping are applied. Scale bar 4 µm. **(D)** Synapses (ROIs) are detected as spherical objects ('spots'). **(E)** Maximum intensity projection of a CA1 pyramidal cell expressing cytosolic mCerulean (inverted gray scale) and postSynTagMA. The cell was stimulated with 50 bAPs at 100 Hz and illuminated with 395 nm (as in Fig. 4). For each identified synapse, $\Delta R/(G_0 + G_1)$ was analyzed, color-coded, and plotted at its original location. Distance from soma is indicated as concentric rings. **(F)** Photoconversion decreased exponentially from the soma with a distance constant of λ = 105 µm (median ± interquartile range, n = 1860 synapses, R^2 = 0.914). **(G)** Spine calcium transient amplitudes during bAP trains (jGCaMP7b) decreased exponentially with distance from the soma with λ = 106 µm, (n = 55 synapses, R^2 = 0.66).

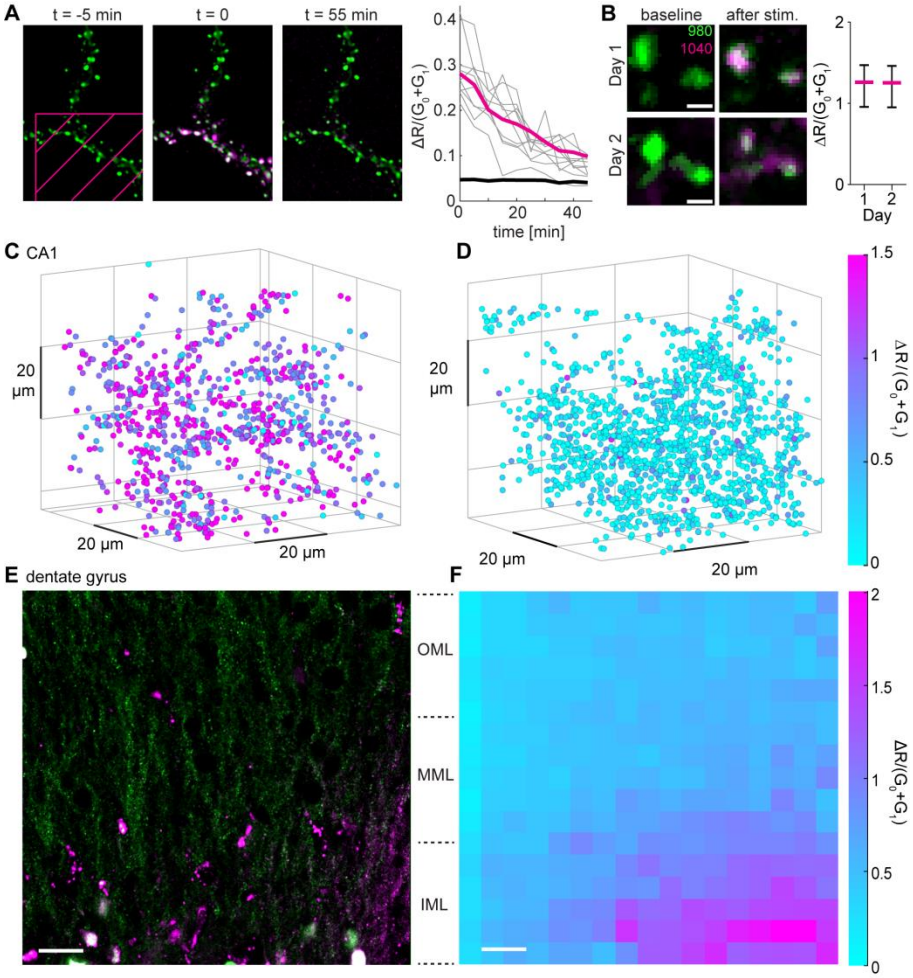

Figure 6 | Using postSynTagMA to map active synapses. (A) Time series of postSynTagMA spots on the dendrite of a cultured neuron. At t = 0, one violet light pulse was applied via DMD inside the hatched area (405 nm, 18.6 mW mm^{-2}, 0.5 s, t = 0 min) while stimulating the culture with a single train of action potentials delivered at 50 Hz for one second. For objects outside the illuminated square, $\Delta R/(G_0+G_1)$ was constant (black line, n = 712, 2 experiments). Inside the illuminated area (magenta line), red fluorescence generated by photoconversion of postSynTagMA decayed exponentially with τ = 29.4 min (R^2 = 0.99, n = 138, 2 experiments). Gray lines show individual examples (n = 1). **(B)** Red/green overlay before and after photoconversion of the same stretch of dendrite on successive days (18 hours between). Suprathreshold extracellular synaptic stimulation was paired with 395 nm light pulses (500 ms, 1s delay, 15x) to photoconvert postSynTagMA (median ± inter-quartile range, n = 37 synapses). Scale bar 1 µm. **(C)** Color-coded $\Delta R/(G_0 + G_1)$ of spines plotted at their location in the 65 x 65 x 78 µm volume of tissue imaged. Suprathreshold stimulation of synaptic inputs in *stratum radiatum* was paired with 395 nm light (100 ms, delay 1s, 50x). Note that $\Delta R/(G_0 + G_1)$ is equal or greater than 1.5 (magenta) for most of the spines (n = 897 synapses). **(D)** As in C) but the extracellular stimulation was subthreshold. Note that $\Delta R/(G_0+G_1)$ is greater than 1 (magenta) for only a few scattered synapses (n = 1502). **(E)** Acute slice of mouse hippocampus expressing postSynTagMA. The tip of a monopolar stimulation electrode was placed in the inner molecular layer (IML) of dentate gyrus, ~40 µm to the right of the image. Green objects (PSDs) were automatically detected and analyzed (n = 19733). Scale bar, 20 µm. **(F)** Average photoconversion of objects in 10 x 10 µm bins. Note that strongly photoconverted objects (magenta) were located in the IML following the axonal projections (horizontal), but not following the dendrites into the outer molecular layer (OML).

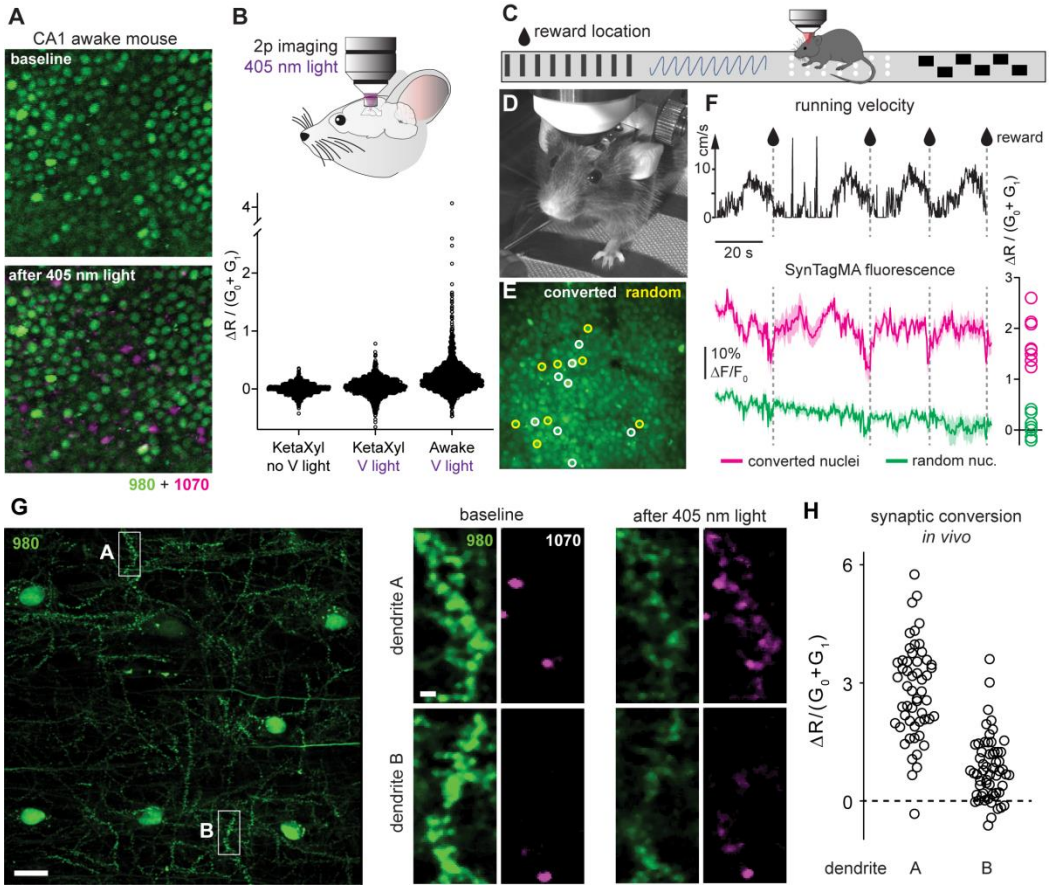

Figure 7 | SynTagMA identifies active neurons during behavior. (A) Nuclei of postSynTagMA expressing CA1 neurons imaged *in vivo* through a chronic cranial window using 980 nm and 1070 nm to excite green and red SynTagMA fluorescence, respectively. Ten 2 s, 405 nm, 12.1 mW mm^{-2} violet light pulses were applied in an awake mouse after which a small percentage of nuclei became photoconverted (magenta). **(B)** Quantification of photoconversion relative to baseline under ketamine-xylazine anesthesia (Keta/Xyl no V light), after 405 nm light as in A (V light) and when the mouse was awake. **(C)** Closed loop paradigm: A head-fixed mouse was trained to stop at a certain position on the running belt to receive a water reward (teardrop). Nuclear fluorescence in CA1 was continuously monitored during 4 laps, followed by 15 laps where 405 nm, 12.1 mW mm^{-2}, 2 s light pulses were triggered together with the water reward. **(D)** Mouse engaged in the task. Note spout for water delivery. **(E)** Two-photon image of CA1 cell body layer during running. Eight nuclei that later became photoconverted are marked by white circles. Yellow circles are the eight randomly selected non-converted nuclei used for comparison of calcium signals. **(F)** Running velocity, corresponding average calcium responses (SynTagMA green fluorescence) of laps 1-4 and subsequent photoconversion of the corresponding eight converted and eight non-converted CA1 nuclei indicated in E. Black trace is running speed during the first 4 laps with times of reward delivery (teardrops/dashed lines). Magenta and green traces are the average green SynTagMA fluorescence of the 8 photoconverted nuclei and the 8 non-converted nuclei, respectively. At right is the photoconversion of the individual nuclei. Note the consistent dips in the magenta trace (i.e. high calcium) just before the water reward/photoconversion light would be triggered. **(G)** PostSynTagMA-expressing interneurons imaged through a chronic cranial window under isoflurane anesthesia. At high magnification, green fluorescence reveals PSD spots on the dendrite. Red spots at baseline are autofluorescent material, not related to SynTagMA. Violet light (20 flashes, 0.2 Hz, 3 s duration, 0.42 mW mm^{-2}) was applied to photoconvert postSynTagMA. Scale bars: 20 µm and 2 µm, respectively. **(H)** Photoconversion of synaptic spots on dendrite A (n = 54) and B (n = 58) indicate higher activity levels in dendrite A.

METHODS

Dissociated rat hippocampal cell cultures

Neurons from P1 Sprague-Dawley rats of either sex were isolated from hippocampal CA1-CA3 regions with dentate gyrus removed, dissociated (bovine pancreas trypsin; 5 min at room temperature), and plated on polyornithine-coated coverslips inside a 6 mm diameter cloning cylinder. Calcium phosphate-mediated gene transfer was used to transfect 5-7 day old cultures. All measurements unless otherwise noted, are from mature 13-21 day old neurons. Procedures with Sprague-Dawley rats were approved by Dartmouth College's Institutional Animal Care and Use Committee (IACUC). Cells were maintained in culture media consisting of Earle's MEM (Thermofisher 51200038), 0.6% glucose, 0.1 g l^{-1} bovine transferrin, 0.25 g l^{-1} insulin, 0.3 g l^{-1} glutamine, 5% fetal calf serum (Atlanta Biologicals), 2% B-27 (Life Technologies), and 4 µM cytosine β-D-arabinofuranoside added 48 hours after plating in 6 mm diameter cloning cylinders (Ace Glass).

Rat hippocampal slice cultures

Hippocampal slice cultures from Wistar rats of either sex were prepared at postnatal day 4–7 as described (Gee et al., 2017). Briefly, rats were anesthetized with 80% CO_2 20% O_2 and decapitated. Hippocampi were dissected in cold slice culture dissection medium containing (in mM): 248 sucrose, 26 $NaHCO_3$, 10 glucose, 4 KCl, 5 $MgCl_2$, 1 $CaCl_2$, 2 kynurenic acid and 0.001% phenol red. pH was 7.4, osmolarity 310-320 (mOsm kg^{-1}), and solution was saturated with 95% O_2, 5% CO_2. Tissue was cut into 400 µM thick sections on a tissue chopper and cultured at the medium/air interface on membranes (Millipore PICMORG50) at 37° C in 5% CO_2. No antibiotics were added to the slice culture medium which was partially exchanged (~60-70%) twice per week and contained (for 500 ml): 394 ml Minimal Essential Medium (Sigma M7278), 100 ml heat inactivated donor horse serum (H1138 Sigma), 1 mM L-glutamine (Gibco 25030-024), 0.01 mg ml^{-1} insulin (Sigma I6634), 1.45 ml 5M NaCl (S5150 Sigma)), 2 mM $MgSO_4$ (Fluka 63126), 1.44 mM $CaCl_2$ (Fluka 21114), 0.00125% ascorbic acid (Fluka 11140), 13 mM D-glucose (Fluka 49152). Wistar rats were housed and bred at the University Medical Center Hamburg-Eppendorf. All procedures were performed in compliance with German law and according to the guidelines of Directive 2010/63/EU. Protocols were approved by the Behörde für Gesundheit und Verbraucherschutz of the City of Hamburg.

Mouse acute hippocampal slices

Male, adult (4-6 months old) C57BL/6J mice were housed and bred in pathogen-free conditions at the University Medical Center Hamburg-Eppendorf. The light/dark cycle was 12/12 h and the humidity and temperature were kept constant (40% relative humidity; 22° C). A bilateral intrahippocampal injection with AAV2/9 encoding syn-postSyntagMA (3.4 x 10^{13} vg ml^{-1}) was administered 7-15 days before acute slice preparation. Mice were anesthetized by CO_2 inhalation, decapitated and brains rapidly removed. Coronal slices (300 µm) were cut on a vibratome (Leica VT1000S) in ice cold solution containing (in mM): 110 choline chloride, 25 $NaHCO_3$, 25 D-Glucose, 11.6 sodium-L-ascorbate, 7 $MgSO_4$, 1.25 NaH_2PO_4, 2.5 KCl, and 0.5 $CaCl_2$. Slices were then incubated at 34° C for 30-45 min in oxygenated acute slice artificial cerebrospinal fluid (ACSF), containing (in mM): 125 NaCl, 26.2 $NaHCO_3$, 11 D-Glucose, 1 NaH_2PO_4, 2.5 KCl, 1.3 $MgCl_2$, and 2.5 $CaCl_2$. Slices were kept in the same solution at room temperature until use.

Anesthetized and awake behaving mice

Male, adult (4-6 months old) C57BL/6J mice were housed and bred in pathogen-free conditions at the University Medical Center Hamburg-Eppendorf. The light/dark cycle was 12/12 h and the humidity and temperature were kept constant (40% relative humidity; 22° C). An AAV2/9 encoding mDlx-postSynTagMA (2.0 x 10^{12} vg ml^{-1}), syn-postSynTagMA (3.4 x 10^{13} vg ml^{-1}) or syn-GCaMP6f (1.45 x 10^{13} vg ml^{-1}) was injected unilaterally in the hippocampus. All procedures performed in mice were in compliance with German law and according to the

guidelines of Directive 2010/63/EU. Protocols were approved by the Behörde für Gesundheit und Verbraucherschutz of the City of Hamburg.

Plasmids

To create preSynTagMA, synaptophysin-GCaMP3 was, as previously described (Hoppa et al., 2012), digested by HindIII and BamHI to remove GCaMP3, and CaMPARI was fused to synaptophysin using the In-Fusion® HD Cloning method and kit (Takara Bio USA) after amplifying variants of CaMPARI with PCR using custom primers with base pair overhangs homologous to the synaptophysin plasmid (3' Primer [CGATAAGCTTTTATGAGCTCAGCCGACC], 5' Primer [CAGATGAAGCTTATGCTGCAGAACGAGCTTG]).

To create postSynTagMA and other related constructs, we followed several steps. After removal of restriction site XbaI from pCAG_PSD95.FingR-eGFP-CCR5TC, PSD95.FingR-eGFP-CCR5TC was inserted into a pAAV-hsyn1 backbone without the CAG promoter or upstream zinc finger binding site, to produce pAAV-syn-PSD95.FingR-eGFP-CCR5TC (available upon request). The eGFP was then replaced with CaMPARI1 (Fosque et al., 2015), from which we had deleted the nuclear export signal (NES), to produce pAAV-syn-PSD95.FingR-dNES-CaMPARI1-CCR5TC, a fusion construct of the fibronectin intrabody and a CaMPARI variant that is not restricted to the cytosol and can enter the nucleus. To finally generate pAAV-syn-postSynTagMA, CaMPARI1 was then replaced by CaMPARI2 (without NES and epitope tags) and the point mutations F391W and L398V were introduced using QuickChange PCR to increase calcium affinity (Moeyaert et al., 2018). The left-handed zinc finger (aka CCR5TC) fused to the KRAB(A) transcriptional repressor (Margolin et al., 1994) was removed to produce pAAV-syn-PSD95.FingR-dNES-CaMPARI2_F391W_L398V, the unregulated variant. A sequence including the zinc finger binding sequence (5'-GTCATCCTCATC-3') (Gross et al., 2013; Perez et al., 2008) upstream of the hsyn1 promoter was synthesized (ThermoFisher) and inserted using the MluI and EcoRI restriction sites to generate pAAV-ZFBS-syn-PSD95.FingR-dNES-CaMPARI2_F391W_L398V-CCR5TC. Other plasmids such as the lower affinity pAAV-syn-PSD95.FingR-dNES-CaMPARI2-CCR5TC, pAAV-syn-synaptophysin-CaMPARI2 and the variants with zinc finger binding sequence are available upon request.

mDlx-postSynTagMA-2A-mCerulean was created by first removing the stop codon from postSynTagMA and inserting a 3'-BsiWI restriction site via PCR. 2A-mCerulean was then inserted 3'of postSynTagMA via Acc65 (5') and HindIII (3') to create postSynTagMA-2A-mCerulean. This construct was subsequently cloned via NheI (5') and BsrGI (3') into the mDlx-GFP-Fishell1 backbone by replacing the GFP with postSynTagMA-2A-mCerulean to generate mDlx-postSynTagMA-2A-mCerulean.

Cell culture imaging

SypCaMPARI experiments (**Fig. 1**) were performed at 34˚ C using a custom-built objective heater. Coverslips were mounted in a rapid-switching, laminar-flow perfusion and stimulation chamber on the stage of a custom-built laser microscope. The volume of the chamber was maintained at ~75 µl and was perfused at a rate of 400 µl min^{-1}. Neurons were perfused continuously during imaging with a standard saline solution containing the following in mM: 119 NaCl, 2.5 KCl, 2 $CaCl_2$, 2 $MgCl_2$, 25 HEPES, 30 D-Glucose, 10 µM CNQX, and 50 µM D-APV. Tetrodotoxin (TTX) was used at a final concentration of 3 µM in standard saline solution during perfusion when noted. Bicuculline was used at a final concentration of 20 µM.

Green fluorescence was measured by illuminating neurons with a 488 nm laser (Coherent OBIS laser, ~ 3 mW) with a ZET488/10x and ZT488rdc dichroic (Chroma). Red fluorescence was measured by illuminating neurons with a 561 nm laser (Coherent OBIS laser) with ZET561/10x and ZT561rdc dichroic (Chroma). All channels were imaged through either a Zeiss EC Plan-Neofluar 40x 1.3 NA objective or an Olympus UAPON40XO340-2 40x 1.35 NA objective. Emission in the green spectra was collected using an ET 525/50m filter (Chroma) and emission in the red spectra was collected using an ET600/50m filter (Chroma). All emission light was collected using an IXON Ultra 897 EMCCD camera (Andor). SypCaMPARI fluorescence was collected with an exposure time of 39.72 ms and images were acquired at 25 Hz.

Cell culture stimulation and photoconversion

Field stimulation-evoked action potentials were generated by passing 1 ms current pulses, yielding fields of ~12 V cm^{-2} through the recording chamber bracketed by platinum/iridium electrodes. Electrical stimuli were locked to start according to defined frame number intervals using a custom-built board named "Neurosync" powered by an Arduino Duo chip (Arduino) manufactured by an engineering firm (Sensostar)(Cho et al., 2017). A collimated 405 nm LED light source (Thorlabs) was set on top of the microscope stage with a custom-built plastic case (Bob Robertson, Dartmouth College). This light source was coupled to a T-Cube LED Driver (Thorlabs) and a Pulse Pal (Open Ephys) was used to trigger light flashes of specific duration and delay. The light source trigger was set relative to a TTL input from Neurosync. Power density of the 405 nm light was measured using a digital handheld optical power and energy meter console with an attached photodiode power sensor (Thorlabs). The power densities used were either 10.8 mW cm^{-2} or 54.1 mW cm^{-2}.

For incubator photoconversion experiments (**Fig. S1**), custom-built circular 51-diode 405 nm LED arrays (Ultrafire) were wired up to a custom dual programmable relay board to flash light for 100 ms every 10 s, inside a cell culture incubator (New Brunswick; Eppendorf) set to ~37˚ C and ~5% CO_2. Neurons were then mounted on the microscope with perfusion, and green fluorescence was imaged during 50 stimulations @ 50Hz (as above) to measure calcium-dependent dimming. Only neurons responsive to stimulation were then analyzed (over ~90% of cells measured).

Patterned time-locking photoconversion

Time locking experiments (Fig. 2) were performed on a Nikon Ti-E microscope fitted with an Andor W1 Dual Camera (Andor CMOS ZYLA), dual spinning disk, Coherent Lasers (OBIS 405, 488 and 561 nm) and the Andor Mosaic 3 micromirror mosaic system, controlled by Andor iQ software, and Nikon elements for image acquisition. A Pulse Pal was used to time lock the stimulus with the mosaic sequence start. A custom 5x5, 250 μm^2 square grid was drawn within the illuminated mosaic field and counterbalanced the different time sequences across various regions of the field.

PSD-95 turnover experiments

PSD-95 turnover experiments were performed on mature neurons (DIV 14-16, 911 days post-transfection). Cells were imaged at ~21˚C in a modified Tyrode's solution containing the following (in mM): 119 NaCl, 2.5 KCl, 3 CaCl2, 1 MgCl2, 25 HEPES, and 30 D-Glucose with 10 µM CNQX. PostSynTagMA photoconversion was induced using a train of 50 action potentials (50 Hz) paired with a 500 ms photoconverting light (18.6 mw mm-2) pulse (500-750 ms delay) in custom-drawn rectangular regions. Z-stacks with a 0.25 µm step size were collected over the course of an hour every 5-6 minutes. Cells were illuminated at each step by 405nm (1% intensity), 488 (25% intensity) and 561 nm (20% intensity) lasers.

Neuron culture image analysis

EMCCD camera images or confocal image stacks were imported into Fiji. A maximum intensity projection was made from the confocal stacks. Ten pixel diameter circular ROIs were placed over boutons identified by eye using a custom written plugin to localize them over the brightest pixel in the green channel (https://imagej.nih.gov/ij/plugins/time-series.html). Boutons were identified as punctate spots that showed a dimming response to AP stimulation (>98% of punctate spots). ROIs were centered on the brightest green pixel in the green channel and average intensity was measured for red and green channels. Average background fluorescence was determined from several larger ROIs placed across the imaging field where there were no transfected axons. The average green and red background fluorescence was subtracted from the respective values before calculating ratios or $\Delta F/F$.

Expression analysis

For each experiment, two groups of six organotypic hippocampal slice cultures (rat) were transduced with 0.5 µl of an AAV2/9 vector (titers were 3.46E+13) with postSynTagMA or the unregulated construct lacking the ZF-KRAB (i.e. from **Fig. 3A**). In the first experiment 7 days elapsed before the slices were pooled and the RNA was extracted and in a second experiment 14 days elapsed. RNA extraction was performed using a GenUP Total RNA kit (biotechrabbit). The samples were homogenized by vigorous shearing of the tissue in 450 µl lysis buffer with 10 strokes of a 1 ml syringe equipped with a 26-gauge canula. Column-based purification was performed according to the instructions given for the kit. Total RNA was eluted in nuclease-free water and photometrically quantified by NanoDrop 2000 (Thermo Fisher Scientific) measurement. Reverse transcription was performed with 500 ng total RNA for each reaction using oligo dT primers as well as hexamer primers of the VILO Mastermix with ezDNase kit (Thermo Fisher Scientific) according to the manufacturer's instructions.

Quantitative PCR analysis

From the rat panels, we selected 48 neuronal, glial and housekeeping genes to be included in a TaqMan Array Plate 48 (Thermo Fisher Scientific) so that two samples could be assayed in parallel on one 96-well plate. The individual targets are listed in **Fig. S2**. Reactions were performed according to the manufacturer's instructions using TaqMan Fast Advanced Master Mix and plates were assayed on an Applied Biosystems 7900 HT Fast Real-Time PCR System (Applied Biosystems, Foster City, CA, USA) in a 96-well format. The following thermal cycling conditions were applied: activation of DNA Polymerase at 95°C for 2 min and two-step cycling with denaturation at 95° C for 2 s, annealing and extension at 60°C for 20 s, and fluorescence data collection run in 40 cycles. Differential gene expression was calculated with the Relative Quantification app (version 3.8, Thermo Fisher).

Propidium Iodide staining

Organotypic hippocampal slices aged between DIV 18-28 were used. 2-4 days before staining, CA1 neurons were electroporated with mCerulean (20 ng μl^{-1}) and postSynTagMA (20 ng μl^{-1}). Slices were placed in the two-photon imaging chamber in HEPES-buffered solution containing 3 µM propidium iodide (PI). The objective was then placed above the CA1 region of the slice and illuminated with violet light (405 nm, 16mW mm^{-2}). Following illumination, slices were kept in the PI solution for 30-45 minutes and subsequently imaged using the 840 nm laser wavelength. PI related photon-emission was collected using 607/70 filters and mCerulean related photon emission was collected using 525/50 filters. NMDA excitotoxicity was used as a positive control. Slices were exposed to 1mM NMDA in HEPES-buffered solution for 1.5 hours and then labeled with PI for 30-45 minutes before imaging as above. To quantify violet light toxicity, PI-positive nuclei were counted in each 2P image stack (background subtracted, median filtered) and were calculated as number of nuclei per volume of tissue.

Single cell electroporation

At DIV 13-17, CA1 neurons in rat organotypic hippocampal slice culture were transfected by single-cell electroporation (Wiegert et al., 2017). Thin-walled pipettes (~10 MΩ) were filled with intracellular K-gluconate based solution into which SynTagMA plasmid DNA was diluted to 20 ng μl^{-1}. In some experiments, a plasmid encoding mCerulean was also included in the pipette at 20 ng μl^{-1}. To enable blind analysis of neurons with and without SynTagMA, the electroporation mixes were coded by a second lab member and only after all recordings and analysis were completed was the investigator unblinded. The intracellular solution contained in (mM): 135 K-gluconate, 4 $MgCl_2$, 4 Na_2-ATP, 0.4 Na-GTP, 10 Na_2-phosphocreatine, 3 sodium-L-ascorbate, 0.02 Alexa Fluor 594, and 10 HEPES (pH 7.2). Pipettes were positioned against neurons and DNA was ejected using an Axoporator 800A (Molecular Devices) with 50 hyperpolarizing pulses (-12 V, 0.5 ms) at 50 Hz.

Two-Photon microscopy in hippocampal slices

Two photon imaging was performed in virally transduced mouse acute hippocampal slice and rat organotypic hippocampal slice cultures 3-4 days after electroporation (DIV 16-20). The custom-built two-photon imaging setup was based on an Olympus BX51WI microscope equipped with LUMPlan W-IR2 60× 0.9 NA (Olympus), W

Plan-Apochromat 40× 1.0 NA (Zeiss) or IRAPO 25x 1.0 NA (Leica) objectives controlled by the open-source software package ScanImage (Pologruto et al., 2003). Two pulsed Ti:Sapphire lasers (MaiTai DeepSee, Spectra Physics) controlled by electro-optic modulators (350-80, Conoptics) were used to excite SynTagMA green (980 nm) and red species (1040 nm), respectively. When Z-stacks of SynTagMA-expressing neurons were acquired, each plane was scanned twice, using 980 nm and 1040 nm excitation, respectively. For quantification of pre- or postsynaptic targeting, axons of CA3 cells or oblique dendrites of CA1 neurons expressing mCerulean and SynTagMA were imaged in *stratum radiatum* at 840 nm and 980 nm, respectively. For three-color experiments, separate stacks were taken to image mCerulean (840 nm) and SynTagMA (980 nm & 1040 nm). Emitted photons were collected through the objective and oil-immersion condenser (1.4 NA, Olympus) with two pairs of photomultiplier tubes (H7422P-40, Hamamatsu). 560 DXCR dichroic mirrors and 525/50 and 607/70 emission filters (Chroma Technology) were used to separate green and red fluorescence. Excitation light was blocked by short-pass filters (ET700SP-2P, Chroma). Two brief violet light pulses (395 nm, 100 ms, 16 mW mm^{-2}, 0.1 Hz) were delivered through the objective using a Spectra X Light Engine (Lumencor) just before imaging to photoswitch the CaMPARI moiety into its bright state (Fosque et al., 2015).

Electrophysiology

Hippocampal slice cultures were placed in the recording chamber of the two-photon laser scanning microscope and continuously perfused with an artificial cerebrospinal fluid (ACSF) saturated with 95% O_2 and 5% CO_2 consisting of (in mM): 119 NaCl, 26.2 $NaHCO_3$, 11 D-glucose, 1 NaH_2PO_4, 2.5 KCl, 4 $CaCl_2$, 4 $MgCl_2$. (pH 7.4, 308 mOsm) at room temperature (21-23° C) or with a HEPES-buffered solution (in mM): 135 NaCl, 2.5 KCl, 10 Na-HEPES, 12.5 D-glucose, 1.25 NaH_2PO_4, 4 $CaCl_2$, 4 $MgCl_2$ (pH 7.4). Whole-cell recordings from CA1 pyramidal neurons were made with patch pipettes (3–4 MΩ) filled with (in mM): 135 K-gluconate, 4 $MgCl_2$, 4 Na_2-ATP, 0.4 Na-GTP, 10 Na_2-phosphocreatine, 3 sodium-L-ascorbate, and 10 HEPES (pH 7.2, 295 mOsm kg^{-1}). Series resistance was below 20 MΩ. A Multiclamp 700B amplifier (Molecular Devices) was used under the control of Ephus (Suter et al., 2010) software written in Matlab (The MathWorks). When using somatic current injection to evoke action potentials in SynTagMA-expressing neurons, the antagonists CPPene (10 µM) and NBQX (10 µM) were added to the extracellular recording solution to block synaptic transmission. For extracellular synaptic stimulation, a monopolar electrode was placed in *stratum radiatum* and two 0.2 ms pulses, 40 ms apart, were delivered using an ISO-Flex stimulator (A.M.P.I.). Stimulation intensity was adjusted to be subthreshold for action potentials (i.e. to evoke ~15 mV EPSPs or ~-500 pA EPSCs) or suprathreshold (i.e. evoking action potentials) by patching a nearby neuron in CA1. To optically stimulate ChR2-expressing CA3 neurons we used a micromanipulator to position the end of a fiber-optic cable to illuminate the CA3 neurons with blue light.

Recording and analysis of miniature EPSCs

CA1 pyramidal neurons expressing mCerulean alone or mCerulean plus SynTagMA were patched 3-5 days after electroporation (see above) using only the mCerulean fluorescence to identify them blind to the conditions. Tetrodotoxin 1 µM, CPPene 1-10 µM, and picrotoxin 50 µM were added to ACSF (see above). Recording electrodes (3-4 MΩ) contained (in mM) 135 Cs-$MeSO_4$, 4 $MgCl_2$, 4 Na_2-ATP, 0.4 Na-GTP, 10 Na_2-phosphocreatine, 3 sodium-L-ascorbate, 10 HEPES (pH 7.2, 295 mOsm kg^{-1}). Series resistance was below 20 MΩ. After the slice rested at least 15 min in the bath, cells were patched and held at -70 mV in the whole-cell voltage clamp configuration (liquid junction potential was not corrected). Currents recorded from 5-15 minutes after break-in were analyzed. The Event Detection feature of Clampfit 10 (Molecular Devices) was used to detect and measure the mEPSC amplitudes and inter-event intervals.

Recording and analysis of cellular parameters

Three to five days after electroporation, CA1 neurons expressing either mCerulean or mCerulean plus SynTagMA, were identified using mCerulean fluorescence and patched in ACSF (see above) supplemented with NBQX 10 µM, CPPene 1 µM, and picrotoxin 50 µM. Recording electrodes contained K-gluconate solution (see

Electrophysiology above). Series resistance was below 20 MΩ. Membrane resistance (R_m) and capacitance (C_m) was calculated by Ephus using -5 mV voltage steps (50 ms) from a holding potential of -70 mV. In the current clamp mode, resting membrane voltage was measured. A 1 second current ramp from 0 to +600 pA was injected to measure the rheobase and the voltage threshold for action potentials. Firing rates were calculated from 1 s current steps from -400 pA to +600 pA.

Ex-vivo stimulation of dentate gyrus

Whole-cell patch clamp recordings from granule cells in dentate gyrus were made at room temperature in acute slice ACSF containing 100 µM picrotoxin to block GABA(A)-dependent inhibitory currents. Borosilicate pipettes (3-6 MΩ) were filled with (in mM): 135 K-gluconate, 4 $MgCl_2$, 4 Na_2-ATP, 0.4 Na-GTP, 10 Na_2-phosphocreatine, 3 sodium-L-ascorbate, and 10 HEPES (pH 7.2, 295 mOsm kg^{-1}). A Multiclamp 700B amplifier (Molecular Devices) was used under the control of Wavesurfer software written in Matlab (The MathWorks). To stimulate axons, a monopolar glass electrode controlled by a stimulus isolator (ISO-flex, AMPI instruments) was placed in the inner molecular layer. Using paired pulse stimulation, (0.2 ms, 40 ms ISI), the stimulation was set just below action potential firing. For photoconversion, 20 pulses (0.2 ms duration, 40 Hz) were used as stimulus and paired with 500 ms violet light (395 nm) 1 second after the start of the stimulation. The protocol was repeated 15 times at 0.1 Hz.

Spine density measurements

Two photon microscopy (840 nm) was used to exclusively excite mCerulean, 3-5 days after electroporation of mCerulean or mCerulean plus SyntagMA as above. A 60X Olympus 1.1 NA collar-corrected water immersion objective (PSF size: 0.35 x 0.35 x 1.5 µm) was used. Z-stacks (0.3 µm z-step) of *stratum radiatum* proximal oblique dendrites (~100 µm from soma) were collected and later deconvolved using a blind deconvolution algorithm in Autoquant X3 (Media cybernetics). Spines and dendrites were semi-automatically detected using the Filament tracer feature of Imaris (Oxford Instruments). For each neuron, spine density (per 10 µm) from 1-3 dendrites of 30-100 µm length was determined.

Photoconversion in hippocampal slice cultures

Photoconversion was achieved by delivery of violet light (duration 100 ms – 2 s as indicated in figure legends, 395 nm, 16 mW mm^{-2}) using a Spectra X Light Engine (Lumencor) coupled with an optical fiber to the epifluorescence port of the two-photon microscope. During the violet light pulses, shutters (Uniblitz) protected the photomultiplier tubes. We typically used 100-500 ms violet light pulses repeated 15-50 times with a 1 s delay from stimulus onset to photoconvert postSynTagMA. An image stack was always taken prior to and following photoconversion. In the bAP experiments, we acquired the first image stack before patching the SynTagMA neuron. The cell was then whole-cell patch-clamped and bAPs (100 Hz) were evoked by somatic current injection and paired with photoconversion light. While acquiring the second image stack, the cell was held in voltage clamp at -65 mV to prevent further action potentials. To monitor turnover of photoconverted SynTagMA, a monopolar glass electrode filled with ACSF was placed in *stratum radiatum* to strongly stimulate synapses onto CA1 postSynTagMA-expressing neurons (100 pulses of 0.2 ms duration, at 100 Hz). Stimulation intensity was adjusted to induce spiking in a neighboring post-synaptic cell. Photoconversion was achieved by delivery of violet light (395 nm, 2 s, 16 mW mm^{-2}) with a 1 s delay from stimulus onset. For relabeling experiments, paired-pulse electrical stimulation (0.2 ms pulses, 40 ms apart) was combined with 250 ms of violet light. This was repeated 25 times at 5 s intervals and a second image stack was acquired immediately thereafter. After imaging, slices were returned to the incubator. About 18 h later, the same procedure was repeated.

Optogenetic stimulation

An AAV2/9 synapsin-ChR2(ET/TC)-2A-synaptophysin-mCerulean, prepared at the UKE vector facility, was injected locally into CA3 of slice cultures at DIV 7. Additionally, several CA1 neurons were electroporated with postSynTagMA (20 ng μl^{-1}) at DIV 22. After allowing 3 days for expression, CA3 neurons were stimulated with blue light pulses (470 nm, 2 pulses, 2-5 ms duration, 40 ms apart) applied through a light fiber positioned under the objective pointed towards CA3. The light intensity and pulse width were set to evoke EPSCs (0.5 – 1.0 nA) in a CA1 neuron close to the postSynTagMA expressing neurons. Pairing stimulation with violet light (1 s delay, 395 nm, 100 ms, 16 mW mm^{-2}) was repeated 50 times at 0.1 Hz to photoconvert postSynTagMA in active spines. Green/red interleaved z-stacks of spiny dendrites were acquired before and after photoconversion. The third z-stack to image the mCerulean labelled boutons was acquired immediately after the post-photoconversion stack.

3D image analysis with manual ROI selection

A macro written in Fiji (Schindelin et al., 2012) was used for two-photon 3D image analysis at 840, 980 and/or 1040 nm wavelengths. When z-stacks contained alternating images collected at 2 excitation wavelengths, they were first separated and then xyz-aligned to correct for chromatic aberration using green and/or red channels and the pairwise stitching plugin (Preibisch et al., 2009). mCerulean and SynTagMA fluorescence values were obtained from images after median filtering and rolling ball background subtraction (Sternberg, 1983). Regions of interest (ROI) were drawn onto maximum intensity projections and compared to axonal or dendrite shafts, respectively. Only spines projecting laterally from the dendrite were analyzed.

For the initial characterization of postSynTagMA, quantification of green to red conversion was performed manually in a small sets of synapses (<50) in Matlab and/or Fiji. Covering relative larger areas of the dendritic tree gave rise to larger data sets (>1000 synapses) that made a semi-automated analysis approach necessary. After rigid registration performed using the Pairwise stitching plugin (Preibisch et al., 2009) in Fiji, 2P images were further processed using a blind deconvolution algorithm in Autoquant X3. Particularly critical was to correct for position change of synapses in 3D due to tissue deformation ("warping") between acquisitions of images, i.e. pre- and post- violet light application. To correct for tissue warping, synapse voxels were reassigned to their initial position using either elastix (Klein et al., 2010) or ANTs (Advanced Normalization Tools, (Avants et al., 2011)). Synapse detection in 2P z-stacks was performed using the Imaris 3D spot detection feature using the G_0 deconvolved signal. Imaris 'Spots' were then used as volumetric ROIs to extract fluorescence values from green and red channels (maximum pixel values from raw images, median filtered) at every time point. Green (G_0 and G_1) and red (R_0 and R_1) values used to quantify photoconversion were normalized to the population mean of G_0 and R_0, respectively.

Automated segmentation and analysis of SynTagMA

To analyze thousands of synapses in large 3D datasets, we developed a pipeline to automatically identify spots in 3D and define volumes (ROIs) for accurate measurements of fluorescence changes. We start with two microscope-specific pre-processing steps followed by SynapseLocator routines, a GUI written in Matlab, which calls specific subroutines (Fiji, elastix, Weka) to perform the analysis:

1. De-interleaving 980/1040 nm image stacks to separate green and red channel
2. Rigid registration to correct for chromatic aberration and beam misalignment
3. Deconvolution and registration of post-image to pre-image using elastix
4. Random forest model, built with machine learning
5. Program identifies spots, determines positions, checks sizes, and creates ROIs
6. Use change in pre/post fluorescence of SyntagMA in ROIs to indicate active spots

A specific challenge was posed by local movements of individual synapses between the time points of data acquisition, which made *post hoc* alignment and de-warping of images an essential step prior to segmentation. A typical experiment consisted of at least two time points (before / after stimulation) in which green and red fluorescence was collected near-simultaneously, alternating between 980 and 1040 nm excitation at every

optical section of the z-stack. For each time point, we corrected channel misalignment due to chromatic aberration by performing rigid registration of the de-interleaved two-color images in Matlab. The detailed workflow in SynapseLocator consists of an initial deconvolution step (Fiji, DeconvolutionLab2 plugin (Sage et al., 2017)) in which diffraction-induced blurring of the images was reduced. We used elastix (Klein et al., 2010) to register image stacks across time points (only green channel; G_0 and G_1). Registration proceeds in four steps (rigid transformation, rotation transformation, affine transformation, and non-rigid registration) for which we provide optimized parameter sets. The transformation was then applied to both red and green channel data (deconvolved and raw). Synapse detection involved a machine learning process accessed via Fiji (Weka, Trainable Weka Segmentation plugin (Arganda-Carreras et al., 2017)). Two classes are manually identified ("spot", "no spot") to train a random forest model considering a set of scale-invariant image features (Hessian and Laplacian, each calculated at three scales, Fiji, FeatureJ plugin). Typically, the model was robust enough to allow for analysis of all experiments from a series. A synapse is identified as a region in which a group of voxels with spot class properties shows minimal connectivity (26-connected neighborhood). For each region, an ellipsoid enclosing the identified connected voxels is calculated in Matlab and stored as ROI. Regions are further filtered by size to exclude objects with extreme values. Inclusion criteria for synapses are: green initial signal (G_0) above background, red initial signal (R_0) below red background, high shape correlation between G_0 and R_1. Converted synapses are identified according to their "conversion-factor" (ΔR / (G_0+G_1)).

Distance-dependence of bAP-induced calcium transients

CA1 neurons expressing mCerulean and postSynTagMA were used for these experiments. Prior to patching the neurons, two z-stacks were acquired along the apical dendritic tree to image mCerulean (840 nm) and postSynTagMA (980 nm / 1040 nm). Each 1024 x 1024 pixel z-stack covered a 150 µm x 150 µm area with depths varying between 50-100 µm. Two to three stacks were required to image the apical dendritic tree. The time taken to image all stacks was 30-40 minutes. After acquiring the first series of images, the cell was whole-cell patch-clamped and 50 back-propagating action potentials (bAPs) were paired with 500 ms violet light (395 nm, 16 mW mm^{-2}, 1 s delay). This pairing was repeated 15 times (0.1 Hz). Immediately after, all 980/1040 nm image stacks were acquired.

In CA1 neurons expressing jGCaMP7b, frame scans (6x6 µm) of oblique dendrites along the entire dendritic arbor were acquired (980 nm) while evoking 50 bAPs (100 Hz) with somatic current injection. In each trial, 50 frames (64 x 64 pixels) were acquired at 5.9 Hz. At least 3 trials were recorded from each section of dendrite. Following calcium imaging, the morphology of the entire cell was imaged using jGCaMP7b baseline fluorescence. The fluorescence time course was measured by placing ROIs on individual spines in Fiji. We calculated $\Delta F/F_0$; F_0 was determined 300 ms prior to bAP onset. To analyze photoconversion (postSynTagMA) or calcium transients (jGCaMP7b) in synapses as a function of distance from the soma, we created a series of 20 µm wide concentric rings around the soma using a custom-written MATLAB script. For the synapses located in each ring, we calculated the median photoconversion (or median calcium transient amplitude) and interquartile range.

Virus injection and hippocampal window surgery

In *ex vivo* experiments (**Fig. 6**), mice were injected with AAV2/9 encoding syn-postSynTagMA (3.4 x 10^{13} vg ml^{-1}) and sacrificed for acute slice preparation 7-15 days after injection. For in vivo imaging experiments (**fig. 7**), mice were injected with an AAV2/9 encoding mDlx-postSynTagMA (2.0 x 10^{12} vg ml^{-1}) or syn-postSynTagMA (3.4 x 10^{13} vg ml^{-1}). *Surgery:* For *ex vivo* experiments, mice received a subcutaneous injection of buprenorphine (0.05 mg kg^{-1} bodyweight) before receiving isoflurane anesthesia (1.5%, mixed in O_2). For *in vivo* experiments, mice were anesthetized with an intraperitoneal injection of Ketamine/Xylazine (0.13/0.01 mg g^{-1} bodyweight). Once mice were anesthetized, they were placed on a heating blanket to maintain the body temperature. In addition, mice received a subcutaneous dose of Carprofen (4 mg kg^{-1}) for post-surgery analgesia. Eyes were covered with eye ointment (Vidisic, Bausch + Lomb) to prevent drying. Prior to surgery, the depth of anesthesia and analgesia was evaluated with a toe-pinch to test the paw-withdrawal reflex. Subsequently, mice were fixed in a stereotactic

frame, the fur was removed with a fine trimmer and the skin of the head was disinfected with Betaisodona solution using sterile cotton swabs. The skin was removed by a midline scalp incision (1-3 cm), the skull was cleaned using a bone scraper (Fine Science Tools) and a small hole was drilled with a dental drill (Foredom) above the injection site. *Injection sites:* For ex vivo experiments, AAV2/9-hSyn-postSynTagMA was injected bilaterally in dentate gyrus targeting -2.2 anteroposterior (AP), +-1.37 mediolateral (ML) and -1.9 dorsoventral (DV) from Bregma. For each side, 500nl were injected. For *in vivo* experiments, AAV2/9-mDlx-SynTagMA-2A-mCerulean or AAV2/9-syn-GCaMP6f was targeted unilaterally to the dorsal CA1 area (− 2.0 mm AP, ± 1.3 mm ML, − 1.5 mm DV relative to Bregma. 0.6 µl of virus suspension was injected. All injections were done at 100 nl min^{-1} using a glass micropipette. After the injection, the pipette stayed in place for at least 5 min after virus delivery before it was withdrawn and the scalp was closed with sutures. During the two days following surgery animals were provided with Meloxicam mixed into soft food.

For *in vivo* experiments, 2 weeks after virus injection, mice were anesthetized by the same procedure as described above to implant the hippocampal window. After fur removal, skin above the frontal and parietal bones of the skull was removed by one horizontal cut along basis of skull and two rostral cuts. The skull was cleaned after removal of the periosteum, roughened with a bone scraper and covered with a thin layer of cyanoacrylate glue (Cyano Veneer). After polymerization a 3-mm circle was marked on the right parietal bone (anteroposterior, −2.2 mm; mediolateral, +1.8 mm relative to bregma) with a biopsy punch and the bone was removed with a dental drill (Foredom). The bone fragment and dura were carefully removed with fine surgical forceps. The cortex above the hippocampus was aspirated with a 0.8 mm blunt needle connected to a water jet pump. When first layer of fibers running orthogonal to midline became visible, a 0.4 mm blunt needle was used to carefully remove the upper two of three fiber layers of the external capsule. Absorbable gelatin sponges (Gelfoam, Pfizer) were used to control bleeding. The craniotomy was washed with sterile PBS and a custom-built imaging window was inserted over the dorsal hippocampus. The window consisted of a hollow glass cylinder (diameter: 3 mm, wall thickness: 0.1 mm, height: 1.5 mm) glued to a No. 1 coverslip (diameter: 3mm, thickness: 0.17 mm) on the bottom and to a stainless steel rim on the top with UV-curable glass glue (Norland NOA61). The steel rim and a head holder plate (Luigs & Neumann) were fixed to the skull with cyanoacrylate gel (Pattex). After polymerization, cranial window and head holder plate were covered with dental cement (Super Bond C&B, Sun Medical) to provide strong bonding to the skull bone. During the two days following surgery animals were provided with Meloxicam mixed into soft food.

Hippocampal imaging and photoconversion *in vivo*

Mice were anesthetized with isoflurane at a concentration ranging between 2.0% and 2.5% in 100% O_2, fixed under the microscope at the head holder plate (Luigs & Neumann) and placed on a heating blanket to maintain the body temperature. Eyes were covered with eye ointment (Vidisic, Bausch + Lomb) to prevent drying. The window was centered under the two-photon microscope (MOM-scope, Sutter Instruments, modified by Rapp Optoelectronics) using a low-magnification objective (4x Nikon Plan Fluorite) and reporter expression (postSynTagMA or GCaMP6f) was verified in the hippocampus using epi fluorescence. The cranial window was then filled with water to image in two-photon mode through a 40x objective (40X Nikon CFI APO NIR, 0.80 NA, 3.5 mm WD). The green species of SynTagMA or GCaMP6f was excited with a Ti:Sa laser (Chameleon Vision-S, Coherent) tuned to 980 nm. The red species of SynTagMA was excited with an ytterbium-doped 1070-nm fiber laser (Fidelity-2, Coherent). Single planes (512x512 pixels) were acquired at 30 Hz with a resonant-galvanometric scanner at 29-60 mW (980 nm) and 41-60 mW (1070 nm) using ScanImage 2017b (Vidrio). Emitted photons were detected by a pair of photomultiplier tubes (H7422P-40, Hamamatsu). A 560 DXCR dichroic mirror and 525/50 and 607/70 emission filters (Chroma Technology) were used to separate green and red fluorescence. Excitation light was blocked by short-pass filters (ET700SP-2P, Chroma). Since SynTagMA fluorescence was relatively low, 450 - 1800 frames per optical plane were acquired and averaged. For identification of active CA1 neurons (**Fig 7A-C**), the conversion protocol consisted of 2 s violet light pulses (405 nm, 12.1 mW mm^{-2})

repeated 10 times in awake and ketamine/xylazine anesthetized mice. In awake behaving mice, photoconversion light was triggered upon water reward delivery. Under isoflurane anesthesia (**Fig. 7G**), conversion of active synapses in interneurons was achieved with 20 flashes of 3 s violet light pulses (405 nm, 0.42 mW mm^{-2}). Motion artefacts were corrected with a custom-modified Lucas-Kanade-based alignment algorithm in Matlab.

References

Adam, Y., Kim, J.J., Lou, S., Zhao, Y., Xie, M.E., Brinks, D., Wu, H., Mostajo-Radji, M.A., Kheifets, S., Parot, V., et al. (2019). Voltage imaging and optogenetics reveal behaviour-dependent changes in hippocampal dynamics. Nature *569*, 413–417.

Andresen, V., Pollok, K., Rinnenthal, J.-L., Oehme, L., Günther, R., Spiecker, H., Radbruch, H., Gerhard, J., Sporbert, A., Cseresnyes, Z., et al. (2012). High-Resolution Intravital Microscopy. PLoS One *7*, e50915.

Arganda-Carreras, I., Kaynig, V., Rueden, C., Eliceiri, K.W., Schindelin, J., Cardona, A., and Sebastian Seung, H. (2017). Trainable Weka Segmentation: a machine learning tool for microscopy pixel classification. Bioinformatics *33*, 2424–2426.

Ariel, P., and Ryan, T.A. (2010). Optical mapping of release properties in synapses. Front. Neural Circuits *4*, 18.

Avants, B.B., Tustison, N.J., Song, G., Cook, P.A., Klein, A., and Gee, J.C. (2011). A reproducible evaluation of ANTs similarity metric performance in brain image registration. Neuroimage *54*, 2033–2044.

Bannister, N.J., and Larkman, A.U. (1995). Dendritic morphology of CA1 pyramidal neurones from the rat hippocampus: II. Spine distributions. J. Comp. Neurol. *360*, 161–171.

Berndt, A., Schoenenberger, P., Mattis, J., Tye, K.M., Deisseroth, K., Hegemann, P., and Oertner, T.G. (2011). High-efficiency channelrhodopsins for fast neuronal stimulation at low light levels. Proc. Natl. Acad. Sci. U. S. A. *108*, 7595–7600.

Bewersdorf, J., Pick, R., and Hell, S.W. (1998). Multifocal multiphoton microscopy. Opt. Lett. *23*, 655.

Bohra, A.A., Kallman, B.R., Reichert, H., and VijayRaghavan, K. (2018). Identification of a Single Pair of Interneurons for Bitter Taste Processing in the Drosophila Brain. Curr. Biol. *28*, 847-858.e3.

Bonhoeffer, T., and Yuste, R. (2002). Spine motility. Phenomenology, mechanisms, and function. Neuron *35*, 1019–1027.

Chen, X., Leischner, U., Rochefort, N.L., Nelken, I., and Konnerth, A. (2011). Functional mapping of single spines in cortical neurons in vivo. Nature *475*, 501–505.

Cho, I.H., Panzera, L.C., Chin, M., and Hoppa, M.B. (2017). Sodium Channel β2 Subunits Prevent Action Potential Propagation Failures at Axonal Branch Points. J. Neurosci. *37*, 9519–9533.

Choi, J.-H., Sim, S.-E., Kim, J.-I., Choi, D. Il, Oh, J., Ye, S., Lee, J., Kim, T., Ko, H.-G., Lim, C.-S., et al. (2018). Interregional synaptic maps among engram cells underlie memory formation. Science *360*, 430–435.

Dana, H., Sun, Y., Mohar, B., Hulse, B.K., Kerlin, A.M., Hasseman, J.P., Tsegaye, G., Tsang, A., Wong, A., Patel, R., et al. (2019). High-performance calcium sensors for imaging activity in neuronal populations and microcompartments. Nat. Methods.

Debanne, D., Guerineau, N.C., Gahwiler, B.H., and Thompson, S.M. (1995). Physiology and pharmacology of unitary synaptic connections between pairs of cells in areas CA3 and CA1 of rat hippocampal slice cultures. J Neurophysiol *73*, 1282–1294.

DeNardo, L., and Luo, L. (2017). Genetic strategies to access activated neurons. Curr. Opin. Neurobiol. *45*, 121–129.

Dürst, C.D., Wiegert, J.S., Helassa, N., Kerruth, S., Coates, C., Schulze, C., Geeves, M.A., Török, K., and Oertner, T.G. (2019). High-speed imaging of glutamate release with genetically encoded sensors. Nat. Protoc. *14*, 1401–1424.

Emptage, N., Bliss, T. V, and Fine, A. (1999). Single synaptic events evoke NMDA receptor-mediated release of calcium from internal stores in hippocampal dendritic spines. Neuron *22*, 115–124.

Feinberg, E.H., Vanhoven, M.K., Bendesky, A., Wang, G., Fetter, R.D., Shen, K., and Bargmann, C.I. (2008). GFP Reconstitution Across Synaptic Partners (GRASP) defines cell contacts and synapses in living nervous systems. Neuron *57*, 353–363.

Fischer, M., Kaech, S., Knutti, D., and Matus, A. (1998). Rapid actin-based plasticity in dendritic spines. Neuron *20*, 847–854.

Fosque, B.F., Sun, Y., Dana, H., Yang, C.-T., Ohyama, T., Tadross, M.R., Patel, R., Zlatic, M., Kim, D.S., Ahrens, M.B., et al. (2015). Labeling of active neural circuits in vivo with designed calcium integrators. Science *347*, 755–760.

Francavilla, R., Villette, V., Martel, O., and Topolnik, L. (2019). Calcium Dynamics in Dendrites of Hippocampal CA1 Interneurons in Awake Mice. Front. Cell. Neurosci. *13*, 98.

Golding, N.L., Kath, W.L., and Spruston, N. (2001). Dichotomy of action-potential backpropagation in CA1 pyramidal neuron dendrites. J Neurophysiol *86*, 2998–3010.

Gray, N.W., Weimer, R.M., Bureau, I., and Svoboda, K. (2006). Rapid redistribution of synaptic PSD-95 in the neocortex in vivo. PLoS Biol *4*, e370.

Grewe, B.F., Langer, D., Kasper, H., Kampa, B.M., and Helmchen, F. (2010). High-speed in vivo calcium imaging reveals neuronal network activity with near-millisecond precision. Nat. Methods *7*, 399–405.

Gross, G.G., Junge, J.A., Mora, R.J., Kwon, H.-B., Olson, C.A., Takahashi, T.T., Liman, E.R., Ellis-Davies, G.C.R., McGee, A.W., Sabatini, B.L., et al. (2013). Recombinant probes for visualizing endogenous synaptic proteins in living neurons. Neuron *78*, 971–985.

Holbro, N., Grunditz, A., and Oertner, T.G. (2009). Differential distribution of endoplasmic reticulum controls metabotropic signaling and plasticity at hippocampal synapses. Proc Natl Acad Sci U S A *106*, 15055–15060.

Holbro, N., Grunditz, A., Wiegert, J.S., and Oertner, T.G. (2010). AMPA receptors gate spine Ca(2+) transients and spike-timing-dependent potentiation. Proc Natl Acad Sci U S A *107*, 15975–15980.

Iacaruso, M.F., Gasler, I.T., and Hofer, S.B. (2017). Synaptic organization of visual space in primary visual cortex. Nature *547*, 449–452.

de Juan-Sanz, J., Holt, G.T., Schreiter, E.R., de Juan, F., Kim, D.S., and Ryan, T.A. (2017). Axonal Endoplasmic Reticulum Ca2+Content Controls Release Probability in CNS Nerve Terminals. Neuron *93*, 867-881.e6.

Klein, S., Staring, M., Murphy, K., Viergever, M.A., and Pluim, J. (2010). elastix: A Toolbox for Intensity-Based Medical Image Registration. IEEE Trans. Med. Imaging *29*, 196–205.

Li, Z., and Murthy, V.N. (2001). Visualizing Postendocytic Traffic of Synaptic Vesicles at Hippocampal Synapses. Neuron *31*, 593–605.

Lin, R., Wang, R., Yuan, J., Feng, Q., Zhou, Y., Zeng, S., Ren, M., Jiang, S., Ni, H., Zhou, C., et al. (2018). Cell-type-specific and projection-specific brain-wide reconstruction of single neurons. Nat. Methods *15*, 1033–1036.

Macpherson, L.J., Zaharieva, E.E., Kearney, P.J., Alpert, M.H., Lin, T.-Y., Turan, Z., Lee, C.-H., and Gallio, M. (2015). Dynamic labelling of neural connections in multiple colours by trans-synaptic fluorescence complementation. Nat. Commun. *6*, 10024.

Margolin, J.F., Friedman, J.R., Meyer, W.K., Vissing, H., Thiesen, H.J., and Rauscher, F.J. (1994). Krüppel-associated boxes are potent transcriptional repression domains. Proc. Natl. Acad. Sci. U. S. A. *91*, 4509–4513.

Marvin, J.S., Scholl, B., Wilson, D.E., Podgorski, K., Kazemipour, A., Müller, J.A., Schoch, S., Quiroz, F.J.U., Rebola, N., Bao, H., et al. (2018). Stability, affinity, and chromatic variants of the glutamate sensor iGluSnFR. Nat. Methods *15*, 936–939.

Megías, M., Emri, Z., Freund, T.F., and Gulyás, A.I. (2001). Total number and distribution of inhibitory and excitatory synapses on hippocampal CA1 pyramidal cells. Neuroscience *102*, 527–540.

Miesenbock, G., De Angelis, D.A., and Rothman, J.E. (1998). Visualizing secretion and synaptic transmission with pH-sensitive green fluorescent proteins. Nature *394*, 192–195.

Moeyaert, B., Holt, G., Madangopal, R., Perez-Alvarez, A., Fearey, B.C., Trojanowski, N.F., Ledderose, J., Zolnik, T.A., Das, A., Patel, D., et al. (2018). Improved methods for marking active neuron populations. Nat. Commun. *9*, 4440.

Nikonenko, I., Boda, B., Steen, S., Knott, G., Welker, E., and Muller, D. (2008). PSD-95 promotes synaptogenesis and multiinnervated spine formation through nitric oxide signaling. J Cell Biol *183*, 1115–1127.

Patel, A., and Cox, D. (2017). Behavioral and Functional Assays for Investigating Mechanisms of Noxious Cold Detection and Multimodal Sensory Processing in Drosophila Larvae. BIO-PROTOCOL *7*.

Pologruto, T.A., Sabatini, B.L., and Svoboda, K. (2003). ScanImage: Flexible software for operating laser scanning microscopes. Biomed. Eng. Online *2*, 13.

Preibisch, S., Saalfeld, S., and Tomancak, P. (2009). Globally optimal stitching of tiled 3D microscopic image acquisitions. Bioinformatics

25, 1463–1465.

Sabatini, B.L., Oertner, T.G., and Svoboda, K. (2002). The life cycle of Ca(2+) ions in dendritic spines. Neuron *33*, 439–452.

Sage, D., Donati, L., Soulez, F., Fortun, D., Schmit, G., Seitz, A., Guiet, R., Vonesch, C., and Unser, M. (2017). DeconvolutionLab2: An open-source software for deconvolution microscopy. Methods *115*, 28–41.

Schindelin, J., Arganda-Carreras, I., Frise, E., Kaynig, V., Longair, M., Pietzsch, T., Preibisch, S., Rueden, C., Saalfeld, S., Schmid, B., et al. (2012). Fiji: an open-source platform for biological-image analysis. Nat. Methods *9*, 676–682.

Scholl, B., Wilson, D.E., and Fitzpatrick, D. (2017). Local Order within Global Disorder: Synaptic Architecture of Visual Space. Neuron *96*, 1127-1138.e4.

Soler-Llavina, G.J., and Sabatini, B.L. (2006). Synapse-specific plasticity and compartmentalized signaling in cerebellar stellate cells. Nat Neurosci *9*, 798–806.

Spruston, N., Schiller, Y., Stuart, G., and Sakmann, B. (1995). Activity-dependent action potential invasion and calcium influx into hippocampal CA1 dendrites. Science *268*, 297–300.

Sternberg (1983). Biomedical Image Processing. Computer (Long. Beach. Calif). *16*, 22–34.

Sturgill, J.F., Steiner, P., Czervionke, B.L., and Sabatini, B.L. (2009). Distinct domains within PSD-95 mediate synaptic incorporation, stabilization, and activity-dependent trafficking. J Neurosci *29*, 12845–12854.

Suter, B.A., O'Connor, T., Iyer, V., Petreanu, L., Hooks, B.M., Kiritani, T., Svoboda, K., Shepherd, G.M.G., Connor, T.O., Ascoli, G., et al. (2010). Ephus: multipurpose data acquisition software for neuroscience experiments. Front. Neural Circuits *4*, 1–12.

Svoboda, K., Denk, W., Kleinfeld, D., and Tank, D.W. (1997). In vivo dendritic calcium dynamics in neocortical pyramidal neurons. Nature *385*, 161–165.

Toni, N., Buchs, P.A., Nikonenko, I., Bron, C.R., and Muller, D. (1999). LTP promotes formation of multiple spine synapses between a single axon terminal and a dendrite. Nature *402*, 421–425.

Topolnik, L., and Camiré, O. (2019). Non-linear calcium signalling and synaptic plasticity in interneurons. Curr. Opin. Neurobiol. *54*, 98–103.

Wiegert, J.S., Gee, C.E., and Oertner, T.G. (2017). Single-cell electroporation of neurons. Cold Spring Harb. Protoc. *2017*, 135–138.

Yasuda, R., Sabatini, B.L., and Svoboda, K. (2003). Plasticity of calcium channels in dendritic spines. Nat Neurosci *6*, 948–955.

Yu, Y., Oberlaender, K., Bengtson, C.P., and Bading, H. (2017). One nuclear calcium transient induced by a single burst of action potentials represents the minimum signal strength in activity-dependent transcription in hippocampal neurons. Cell Calcium *65*, 14–21.

Zolnik, T.A., Sha, F., Johenning, F.W., Schreiter, E.R., Looger, L.L., Larkum, M.E., and Sachdev, R.N.S. (2017). All-optical functional synaptic connectivity mapping in acute brain slices using the calcium integrator CaMPARI. J. Physiol. *595*, 1465–1477.